Am J Cancer Res 2024;14(8):4082-4095
www.ajcr.us /ISSN:2156-6976/ajcr0159087

*Original Article*

# RNF26-mediated ubiquitination of TRIM21 promotes bladder cancer progression

Dongwei Yao[1,2*], Feng Xin[2*], Xiaozhou He[1]

*[1]Department of Urology, The Third Affiliated Hospital of Soochow University, Soochow University, Changzhou 213000, Jiangsu, China; [2]Department of Urology, The Second People's Hospital of Lianyungang, Lianyungang 222023, Jiangsu, China. [*]Equal contributors.*

Received July 9, 2024; Accepted August 21, 2024; Epub August 25, 2024; Published August 30, 2024

**Abstract:** RNF26 is an important E3 ubiquitin ligase that has been associated with poor prognosis in bladder cancer. However, the underlying mechanisms of RNF26 in bladder cancer tumorigenesis are not fully understood. In the present study, we found that RNF26 expression level was significantly upregulated in the bladder cancer tissues, and higher RNF26 expression is closely associated with poorer prognosis, lower immune cell infiltration, and more sensitive to immune checkpoint blockade drugs and chemotherapy drugs, including cisplatin, VEGFR-targeting drugs and MET-targeting drugs. RNF26 knockdown in UMUC3 and T24 cell lines inhibited cell growth, colony formation and migratory capacity. Meanwhile, RNF26 overexpression had the opposite effects. Mechanistically, RNF26 exerts its oncogenic function by binding to TRIM21 and promoting its ubiquitination and subsequent degradation. Moreover, we revealed ZHX3 as a downstream target of RNF26/TRIM21 pathway in bladder cancer. Taken together, we identified a novel RNF26/TRIM21/ZHX3 axis that promotes bladder cancer progression. Thus, the RNF26/TRIM21/ZHX3 axis constitutes a potential efficacy predictive marker and may serve as a therapeutic target for the treatment of bladder cancer.

**Keywords:** RNF26, TRIM21, ZHX3, bladder cancer, ubiquitination

## Introduction

Bladder cancer has become the second most common urological cancer, and the incidence and mortality rates are increasing every year [1, 2]. Although the clinical outcomes of bladder cancer have improved significantly with the development of surgical approaches and targeted therapy, the 5-year survival rate for patients with bladder cancer is still unsatisfactory [3]. In addition, bladder cancer tends to have a high rate of postoperative recurrence, possibly due to its multifocal and implantation characteristics [4]. However, the behind mechanisms are still unclear. Therefore, in-depth studies are urgently needed to further our understanding of bladder cancer tumorigenesis and progression and to identify novel diagnostic and therapeutic targets for bladder cancer.

Ubiquitination is an important post-transcriptional modification that can alter protein localization and lead to protein degradation [5]. E3 ubiquitin ligase is the key enzyme for ubiquitination, transferring ubiquitin from the E2 enzyme to the underlying protein [6]. In addition, E3 ubiquitin ligases have been closely associated with tumorigenesis, progression, microenvironment, immunotherapy, and drug resistance in bladder cancer [7], and thus utilization of E3 ubiquitin ligase-targeted drugs has emerged as a novel approach for bladder cancer treatment [8]. ER-embedded RING finger protein 26 (RNF26) is an important E3 ubiquitin ligase that mediates ubiquitination of sequestosome 1 (SQSTM1) by interacting with the ubiquitin-binding enzyme UBE2J1, so as to anchor homologous vesicles in the perinuclear region of the cell and to facilitate the termination of epidermal growth factor (EGF)-induced AKT signaling [9, 10]. RNF26 can also collaborate with vimentin to maintain endoplasmic reticulum architecture and dynamics [11]. Moreover, RNF26 is prevalent in normal human tissues but is upregulated in several human

https://doi.org/10.62347/TECQ5002

tumor cell lines (HL-60, HeLa S3 and SW480) [12]. Studies have shown that RNF26 could promote progression of pancreatic cancer and renal cell carcinoma through degrading RNA binding motif protein-38 (RBM38) and chromobox 7 (CBX7), respectively [13, 14]. Significantly higher expression of RNF26 was detected in bladder cancer cells and tissues, which was significantly associated with poor prognosis. Forkhead box M1 (FOXM1) promotes RNF26 expression at the transcriptional level, and RNF26 degrades p57 (CDKN1C) through a ubiquitination-dependent manner to regulate cell cycle processes [15]. Nevertheless, the relationship between RNF26 and the immune microenvironment of bladder cancer, the effect of chemotherapy, the benefit of immunotherapy, and how ubiquitination of candidate proteins may play a role in the progression of bladder cancer remains unclear.

In this study, we systematically investigated the relationship between RNF26 expression and bladder cancer prognosis and progression, immune microenvironment, chemotherapeutic drug efficacy, as well as the immune checkpoint blockade therapy benefits. The oncogenic effects of RNF26 and the candidate RNF26 binding proteins and their ubiquitination were also explored, suggesting existence of a novel tripartite motif containing 21 (TRIM21)/zinc fingers and homeoboxes 3 (ZHX3) axis in bladder cancer tumorigenesis and progression.

## Materials and methods

### *Bioinformatics analysis*

RNF26, TRIM21 and ZHX3 expression in normal and bladder cancer tissues from TCGA (https://portal.gdc.cancer.gov/). Cases were stratified according to median expression level into high and low expression groups for RNF26, TRIM21, and ZHX3. The relationship between RNF26, TRIM21, and ZHX3 expression and bladder cancer survival outcomes, including overall survival (OS), disease free survival (DFS) and progress free interval (PFI), was analyzed using Kaplan-Meier (KM) survival curve analyses. We also analyzed the differences in infiltration of 22 immune cell types between the two expression groups using the CIBERSORT algorithm based on the LM22 gene signature file [2, 16, 17]. In light of the importance of checkpoint inhibitor-based therapy, the expression patterns of immune checkpoint molecules in the high and low expression groups were further analyzed [18]. The half-maximal inhibitory concentration (IC50) values of each TCGA-bladder cancer sample were assessed using the pRRophetic R package [19], and the IC50 values of different therapeutic agents in the high-risk and low-risk groups were compared using the Wilcoxon signed-rank test to determine the sensitivity of the different expression groups to chemotherapeutic agents [20].

### *Cell culture and transfection*

The human bladder cancer cell lines UMUC3 and T24 were obtained from the Chinese Academy of Cell Collection (Shanghai, China) and cultured in RPMI 1640 medium containing 10% foetal bovine serum, 100 U/ml penicillin-streptomycin, at 37°C under 5% $CO_2$ in a humidified incubator. For cell passages, cells were detached using 0.25% trypsin-EDTA (Invitrogen, USA) for 3-5 minutes at 37°C. The cell suspension was then centrifuged at 300 g for 5 minutes. Cells were counted using a hemocytometer, and the appropriate number of cells were seeded into new culture flasks at a 1:3 ratio. For transient knockdown, small interfering RNAs (siRNAs) (GenePharma, Suzhou, China) and overexpression plasmids (GenePharma) were transfected into UMUC3 and T24 cells with Lipofectamine 2000 (Invitrogen) according to the manufacturer's instructions. The nucleotide sequence of siRNA was as follows: si-NC, 5'-UUCUCCGAACGUGUCAGGU-3'; si-RNF26 1#, 5'-UAGUGAAAUGUGCACAGUCUG-3'; si-RNF26 2#, 5'-UUGAGGUCCAACACCAAGGUC-3'; si-ZHX3, 5'-AUGAUUGUCUGGCUUGGCC-3'. To investigate potential forms of lysine ubiquitination, specifically focusing on the prevalent K48 ubiquitination-mediated protein degradation, T24 cells were transfected with Ub-WT, Ub-K48, Ub-K48R, and Ub-K0 mutants. Cells were harvested for analysis at 48 h post-transfection.

### *RNA extraction and quantitative real-time (qRT)-PCR*

Total RNA was extracted using the RNeasy Plus Micro Kit (Qiagen, Düsseldorf, Germany). RNA was reversely transcribed into cDNA using PrimeScript Reverse Transcription Kit (Vazyme, Nanjing, China). The mRNA expression was quantified on an ABI 7500 Real-Time PCR

System (Applied Biosystems, Foster City, CA, USA) using SYBR Premix Ex Taq polymerase (Takara, Dalian, China). 18S ribosomal (r)RNA was chosen as an internal control and relevant expression was calculated by $2^{-\Delta\Delta Ct}$ method. The following primers were used in the qRT-PCR reaction: RNF26 forward 5'-ACTGAAAT-CCTGATGCGCCA-3' and reverse 5'-ACAGGGGT-AGGAGGGGATTC-3'; and 18S rRNA forward 5'-AAACGGCTACCACATCCAAG-3' and reverse 5'-CCTCCAATGGATCCTCGTTA-3'.

*Cell proliferation, colony formation and migration assays*

Cell viability was measured using the CCK-8 kit (Beyotime, Beijing, China), as previously described [21-24]. The optical density (OD) was measured at 450 nm wavelength using a microplate reader (Bio-Rad Model 680, Richmond, CA, USA). For colony formation, 1000 transfected cells were seeded in 6-well plates and maintained in RPMI-1640 medium containing 10% FBS. After two weeks, cell colonies were fixed with methanol for 15 min and stained with 0.1% crystal violet (Sigma-Aldrich) for 30 min. Subsequently, those visible colonies were photographed and counted using the ImageJ software.

Cell migration assay was performed by a transwell chamber (Corning, USA), as previously described [25-27]. In brief, transfected cells were suspended in 150 μL of serum-free medium and cultured in the upper transwell chamber and the lower chamber was filled with 600 μL of the medium supplemented with 10% FBS. After 48 h of incubation, cells inside the upper chamber were removed using cotton wool, and the cells moving to the lower side were fixed with 4% paraformaldehyde and dyed with 0.1% crystal violet (Beyotime). Finally, five randomly selected fields of view were photographed under an inverted microscope and counted in each well.

*Xenografts assay*

The animal experiments were approved by the Soochow University Animal Ethics Committee. In brief, four-week-old male BALB/c nude mice were maintained in specific pathogen-free (SPF) animal room and manipulated according to protocols. ShRNF26 and negative control shRNA (GenePharma) were stably transfected into UMUC3 cells. The transfected cells were subcutaneously injected into a single side of the posterior flank of each mouse. Tumor growth was examined every 3 days, and tumor volumes were calculated by the equation $V = 0.5 \times D \times d^2$ (V, volume; D, longitudinal diameter; d, latitudinal diameter). After 15 days, mice were euthanized under carbon dioxide exposure followed by cervical dislocation, the subcutaneous tumors were obtained and imaged, and tumor volumes and weight were examined. Tumor cell proliferation was assessed by Ki67 staining. The specimens were fixed with methanol/acetone and incubated with Ki67 antibody (1:200 dilution; Abcam, USA). The percentage of Ki67-positive cells was determined by cell counting at least five microscopic fields of view. This study was carried out in strict accordance with the Guide for the Care and Use of Laboratory Animals of the National Institutes of Health.

*Immunoprecipitation (IP) assays*

Cell lysates were incubated with anti-Flag antibody (Sigma) or anti-GFP antibody (Abcam) for Co-IP experiments as previously described [28]. Briefly, cells were lysed using RIPA lysis buffer (Beyotime, Nantong, China) on ice for 30 min, followed by preclearing with protein A beads (Invitrogen). Lysates were incubated with the indicated primary antibodies or IgG antibody overnight at 4°C, followed by incubation with protein A beads for 3 h at 4°C. The immunoprecipitates were prepared for subsequent western blotting analysis by applying heat (95°C) to the beads with 2× SDS buffer for a duration of 5 minutes.

*Liquid chromatography-tandem mass spectrometry analysis (LC-MS/MS)*

The gel particles were washed sequentially with deionized water, 50% acetonitrile, and 100% ACN. The proteins contained in the gel particles were reduced and alkylated for 45 minutes at room temperature. The gel particles were then washed thoroughly and dried naturally. The gels were hydrated at 4°C for 30 minutes. The gels were then digested at 37°C for 12 hours. All extracts and supernatants were combined and dried using a SpeedVac. The digested peptides were desalted using a StageTip and analyzed using an LTQ Orbitrap Velos mass spectrometer (Thermo Scientific,

Waltham, USA). Tandem mass spectra were searched using the UniProt protein database to identify proteins and peptides using a false discovery rate of 1%. All experiments were performed in triplicate. Protein expression levels were estimated using the iBAQ algorithm embedded in MaxQuant for label-free quantification.

*Protein half-life assay*

After transfection with Empty vector (EV) or pcDNA3.1-RNF26, T24 cells were treated with cyclohexanone (CHX, 100 μg/mL, Sigma) at different time points to block protein synthesis, and proteins were harvested for western blotting analysis to detect TRIM21 at 0, 3, and 6 hours.

*Western blotting*

For western blotting analysis, total protein was extracted from cell lines and tissue samples using RIPA buffer. Proteins were separated by 10% SDS-PAGE electrophoresis according to molecular weight and then transferred to a polyvinylidene difluoride membrane (Millipore, Bedford, MA, USA). Membranes were blocked in Tris-Tween (TBST) containing 5% nonfat dry milk for 1 hour at room temperature and incubated with the indicated primary antibody dilutions (anti-RNF26, 1:1000; anti-TRIM21, 1:1,000; anti-ZHX3, 1:1,000, and anti-tubulin, 1:3,000; all from Proteintech) overnight at 4°C. On the next day, the membranes were washed 3 times for 10 min each and incubated with horseradish peroxidase (HRP)-conjugated secondary antibody for 1 h at room temperature. Protein bands were detected using an enhanced chemiluminescent substrate (Thermo Scientific). In our study, bladder cancer samples and normal tissues for Western blotting were obtained from patients treated for bladder cancer at the Second People's Hospital of Lianyungang between February 2021 and February 2023 and were approved by the Second People's Hospital of Lianyungang's Ethics Committee (2021-007-01).

*Immunofluorescence*

For immunofluorescence, fresh 5 μm slides were obtained from paraffin-embedded bladder cancer and control tissue from xenografts assay. 5% bovine serum albumin (BSA, w/v; Sunshine, Nanjing, China) is used for blocking to reduce non-specific binding of antibodies. The sections were incubated with 100 μl of primary antibody dilutions (anti-ZHX3, Proteintech; anti-TRIM21, Proteintech; anti-Ki67, Abcam) overnight at 4°C. Subsequent, Alexa-Fluor secondary antibodies staining, 4',6-diamidino-2-phenylindole (DAPI) staining, and photographed under a confocal laser microscope (Zeiss LSM710, Carl Zeiss, Oberkochen, Germany).

*Statistical analysis*

Data were analyzed using GraphPad Prism 9.0 (GraphPad, USA) and SPSS 22.0 (IBM, Chicago, IL, USA). Data from at least three independent replicate experiments are presented as mean ± standard deviation (SD). Differences between the two groups, or between more than two groups, were analyzed using Student's t-test or one-way ANOVA [29]. For multiple time points, a Tukey post hoc test following the Repeat measurement ANOVA was adopted to compare the two groups. $P < 0.05$ was set as the threshold for statistical significance.

## Results

*RNF26 expression significantly correlates with prognosis and response to targeted treatment in bladder cancer patients*

To investigate whether RNF26 plays an oncogenic role in bladder cancer progression, RNF26 expression in para-cancerous tissue and tumor tissue was analyzed using TCGA data. RNF26 expression level was significantly upregulated in the bladder cancer tissues compared to para-cancerous tissue (**Figure 1A**). Then, we performed western blotting to detect RNF26 expression in patients with bladder cancer and found that RNF26 significantly overexpressed in bladder cancer tissues compared with normal counterparts (**Figure 1B**, **1C**). KM survival analysis showed that low expression of RNF26 were related to the good overall survival (OS) and disease free survival (DFS) in bladder cancer from TCGA database (**Figure 1D**, **1E**). The 22 immune cell proportions of bladder cancer patients in the RNF26 high- and low-expression groups were quantified by the CIBERSORT algorithm. Compared to high-expression group, B cell memory, B cell plasma, T cell follicular helper, T cell regulatory (Tregs), Monocyte, Myeloid dendritic cell acti-

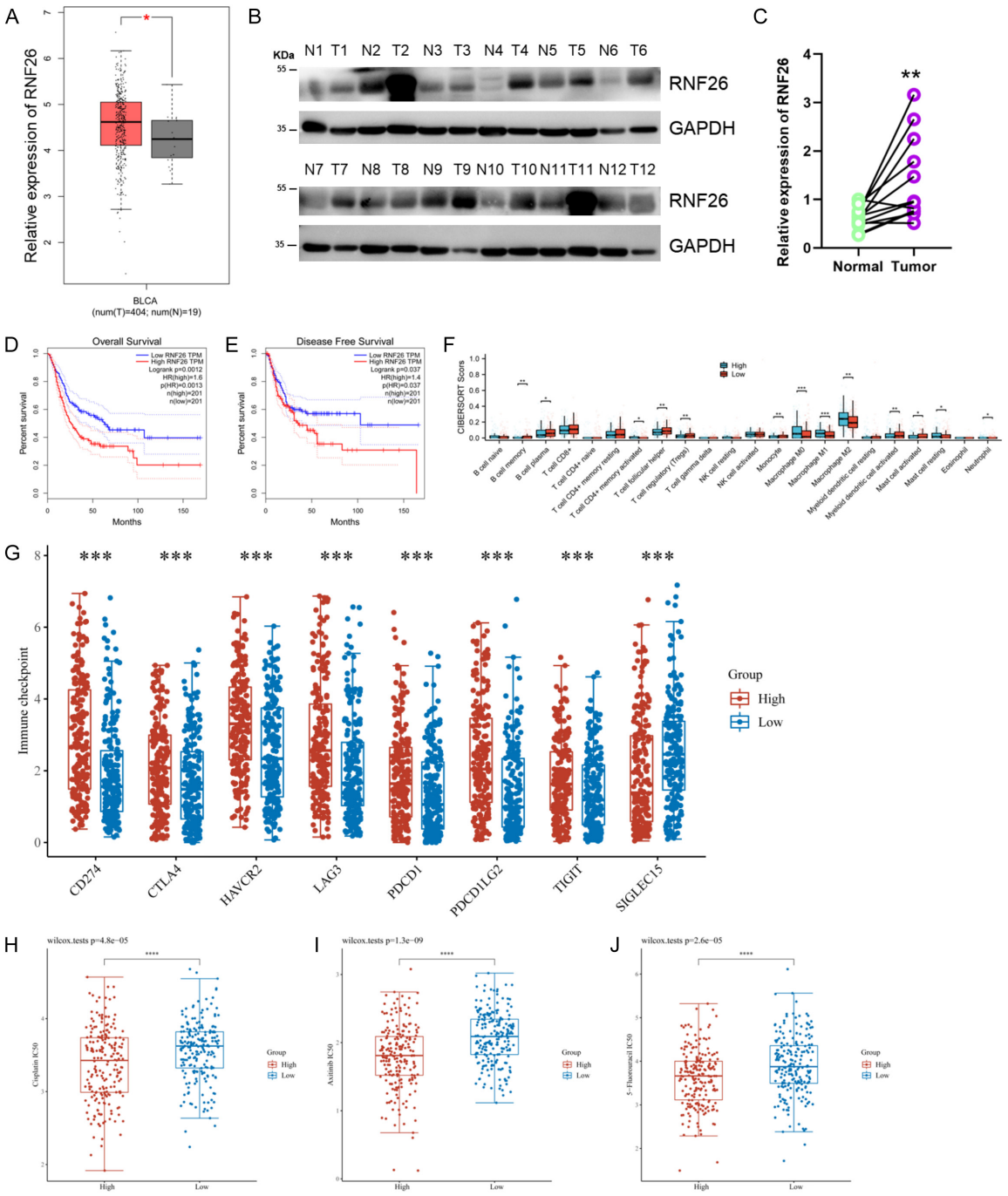


**Figure 1.** RNF26 expression was significantly associated with prognosis and drug sensitivity in patients with bladder cancer. A. RNF26 expression was upregulated in the bladder cancer tissues in TCGA-BLCA dataset. B, C. RNF26 expression in bladder cancer patients using western blotting. D, E. Overall survival (OS) and disease-free survival (DFS) were significantly worse in bladder cancer patients with high RNF26 expression from TCGA database. F. Comparison of immune cell infiltration between the high and low RNF26 expression groups. G. The difference in immune checkpoint molecules between the high and low RNF26 expression groups. H-J. RNF26 high-expression group were more sensitive to cisplatin, VEGFR targeted drugs (Axitinib) and MET targeted drugs (5-Fluorouracil). *P < 0.05; **P < 0.01; ***P < 0.001; ****P < 0.0001.

vated and Mast cell activated significantly higher in low-expression group, whereas T cell CD4+ memory activated, Macrophages M0, Macrophages M1, macrophages M2, Mast cell

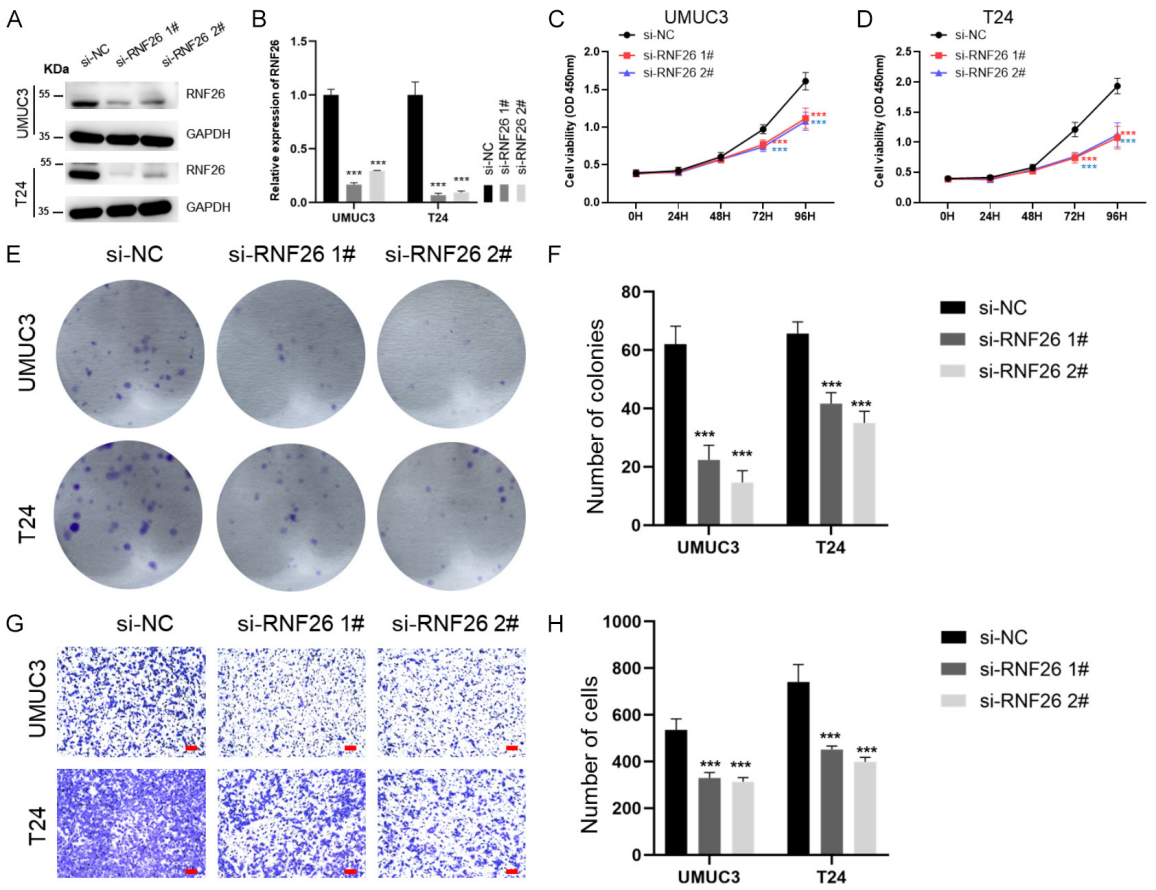


**Figure 2.** Knockdown of RNF26 inhibits bladder cancer cell growth. A, B. Cells were transfected with RNF26-siRNA to knockdown RNF26. C, D. CCK-8 assay indicated that the proliferation of UMUC3 and T24 cells was inhibited following RNF26 knockdown. n = 6 for each group. E-H. Colony formation and migrated cells were significantly reduced in RNF26-siRNA cells compared to control cells. n = 3 for each group. Scale bar: 100 μm. ***P < 0.001.

resting and Neutrophil were significant reduction in low-expression group (**Figure 1F**). Given the importance of checkpoint inhibitor-based therapy, we also compared the expression of immune checkpoint that differed between the two groups. Interestingly, the expression of all checkpoint molecules was remarkably higher in the RNF26 high-expression group than in the low-expression group, except for SIGLEC15 (**Figure 1G**), suggesting that patients in the RNF26 high-expression group may have greater immune escape and better benefit from immunotherapy. To investigate whether the response of chemotherapy correlates with RNF26 expression, the pRRophetic algorithm was performed. The patients of RNF26 high-expression group were more sensitive to cisplatin, VEGFR targeted drugs (Axitinib) and MET targeted drugs (5-Fluorouracil) (**Figure 1H-J**). These results suggest a correlation between RNF26 and bladder cancer pathogenesis and have the potential to serve as a molecular marker to guide chemotherapy and immunotherapy in bladder cancer patients.

*Knockdown of RNF26 inhibits bladder cancer cell growth in vitro and in vivo*

Since the above results suggest that RNF26 is a potential bladder cancer oncogenic protein, we investigated the effect of RNF26 on bladder cancer tumorigenesis. Bladder cancer cell lines T24 and UMUC3 were transfected with si-RNF26, which leads to decreased expression of RNF26 (**Figure 2A**, **2B**). CCK-8 assay results showed that knockdown of RNF26 significantly decreased cell proliferation in a time-dependent manner (**Figure 2C**, **2D**). Colony formation assay and transwell assay explored the effect of RNF26 silencing on clonogenicity and migra-

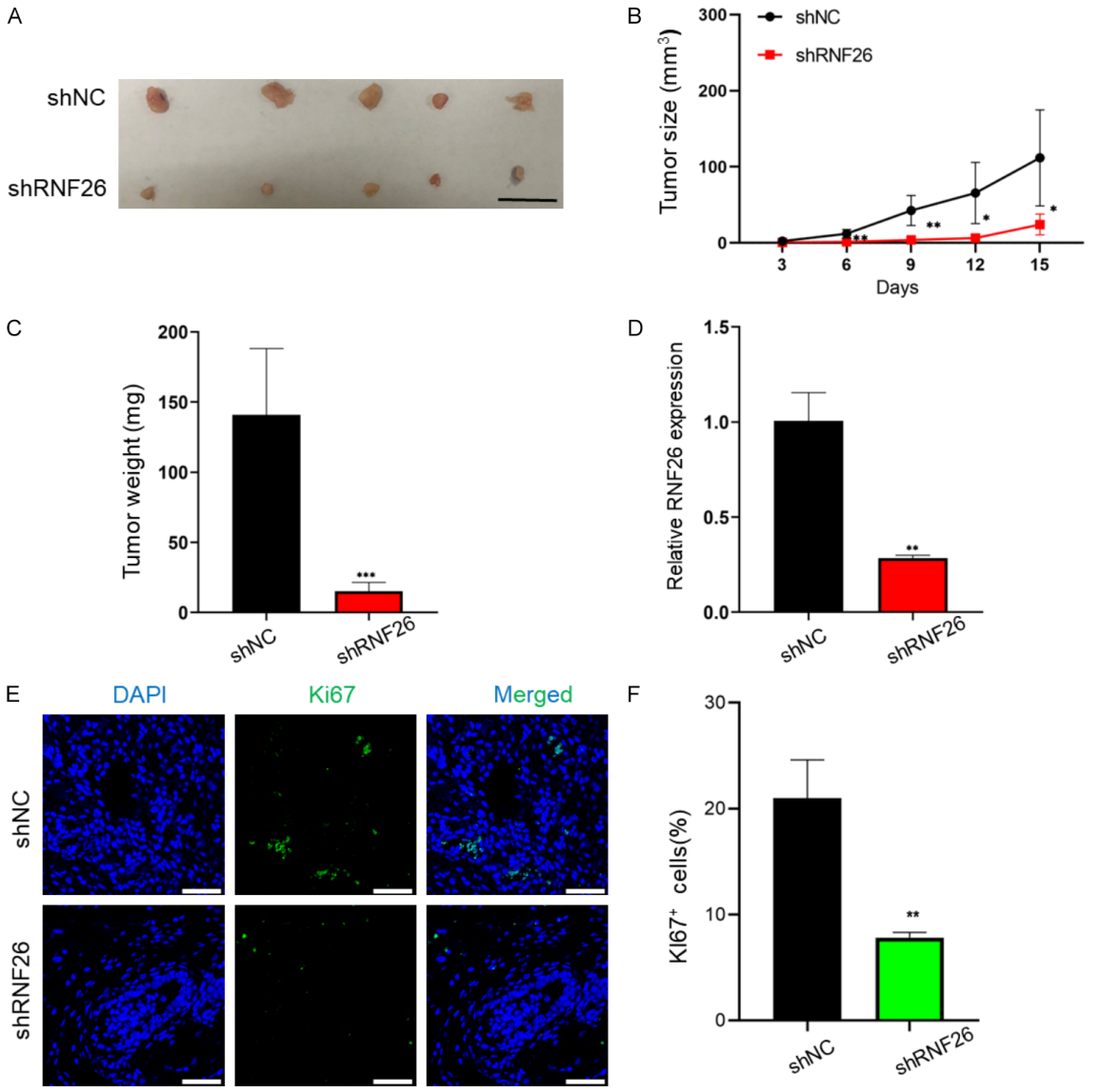


**Figure 3.** Knockdown of RNF26 inhibits bladder cancer cell tumorigenicity in xenograft tumor models. A-C. The tumor sizes and weight of mice were decreased in RNF26 knockdown group. n = 5 for each group. Scale bar: 1 cm. D. Relative expression of RNF26 in tumors transfected with shNC and shRNF26. E, F. Immunostaining of Ki67 indicates that RNF26 knockdown inhibits cell proliferation in xenograft tumor models. n = 5 for each group. Scale bar: 50 μm. *P < 0.05, **P < 0.01, ***P < 0.001.

tion of bladder cancer cells and found that colony formation and migrated cells were significantly reduced in RNF26-siRNA cells compared to control cells (**Figure 2E-H**).

To further determine the role of RNF26 in bladder cancer development, we conducted xenograft assays in nude mice. The results showed that significant downregulation of RNF26 in xenograft tumour models and that RNF26 knockdown inhibited tumor growth and weight (**Figure 3A-D**). Moreover, immunofluorescence staining indicated that Ki67-positive cells were significantly reduced in the RNF26 knockdown group (**Figure 3E**, **3F**), suggesting that knockdown of RNF26 can inhibit bladder cancer cell proliferation in vivo.

*Overexpression of RNF26 promotes bladder cancer cells proliferation and migration*

To further validate the oncogenic effect of RNF26 in bladder cancer, T24 and UMUC3 were transfected with pcDNA3.1-RNF26. CCK-8

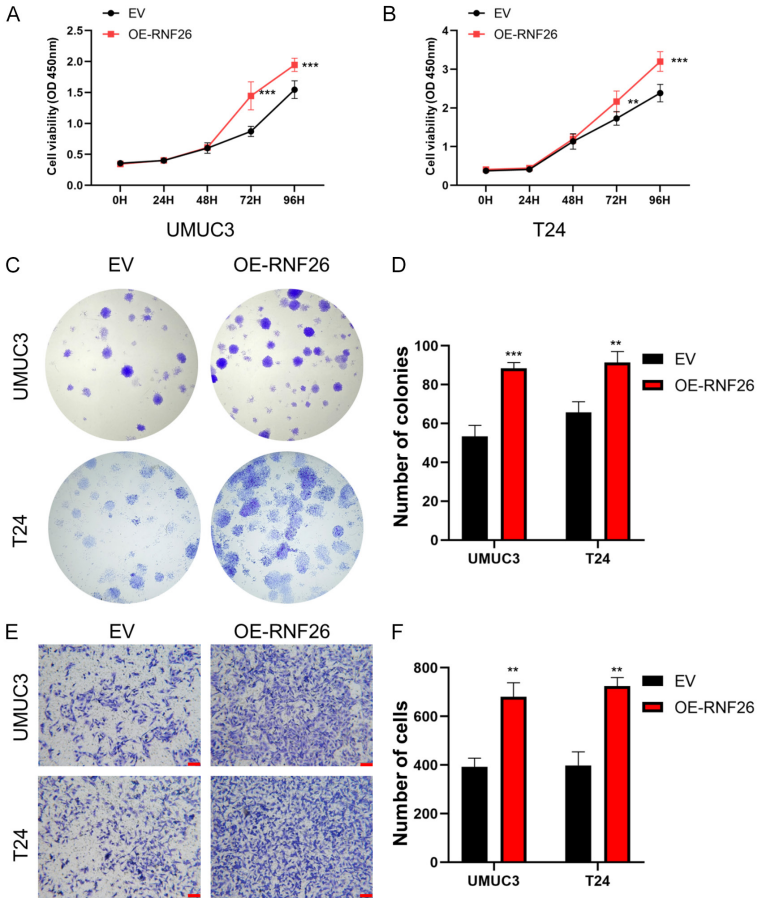


**Figure 4.** Overexpression of RNF26 promoted the malignant level of bladder cancer cells in vitro. A, B. CCK-8 assay indicated that the proliferation of UMUC3 and T24 cells was promoted following RNF26 overexpression. n = 6 for each group. C-F. Clonogenicity and migrated cells were increased in RNF26 overexpression cells compared to control cells. n = 3 for each group. Scale bar: 50 μm. **P < 0.01; ***P < 0.001.

assay was performed and the results showed that overexpression of RNF26 significantly enhanced the growth ability of bladder cancer cells (**Figure 4A**, **4B**). Moreover, colony formation and migrated cells were significantly increased in RNF26-overexpression cells compared to control cells (**Figure 4C-F**).

*RNF26 interacts with TRIM21 and promotes its K48-linked ubiquitination*

To clarify the downstream substracts of RNF26, we performed three independent i immunoprecipitation-liquid chromatography-tandem mass spectrometry (IP-LC-MS/MS) analyses using RNF26 overexpressing T24 bladder cancer cells. As a result, 259 potential target proteins were identified from three independent experiments (**Figure 5A**, **5B**; Table S1). Among them, TRIM21 plays a key regulatory function in bladder cancer progression and is in the TOP10 candidates according to the iBAQ ranking (**Figure 5C**) [30]. Therefore, TRIM21 was selected as a candidate target for RNF26. First, Co-IP experiments were performed to confirm the interaction between RNF26 and TRIM21 (**Figure 5D**). In bladder cancer cells, TRIM21 works as an E3 ligase to mediate ZHX3 ubiquitination and subsequent degradation [30]. We therefore supposed that ZHX3 may be involved in the RNF26/TRIM-21 pathway. Indeed, western blotting results showed that RNF26 overexpressing in T24 and UMUC3 cells reduced TRIM21 protein expression and promotes ZHX3 expression (**Figure 5E**). We also examined TRIM21 and ZHX3 expression following knockdown of RNF26 in the xenograft tumour model described above and found that TRIM-21 expression increased and ZHX3 expression decreased following RNF26 knockdown (**Figure 5F-H**). Cycloheximide (CHX) treatment significantly shortened the half-life of TRIM21 protein and increased the half-life of ZHX3 protein after overexpression of RNF26 in T24 cells (**Figure 5I-K**). Moreover, overexpression of RNF26 increased the level of polyubiquitination of TRIM21 in T24 cells (**Figure 5L**). In particular, the level of polyubiquitination was promoted by the addition of MG132, a well-known proteasome inhibitor. To explore potential lysine ubiquitination types, the most common form of K48 ubiquitination-mediated protein degradation, we subsequently transfected T24 cells with Ub-K48-only, Ub-K48R and Ub-K0 mutants [31]. The results showed that wild-type (WT) Ub and Ub-K48-only could be linked to TRIM21 by RNF26, suggesting that RNF26 promoted K48-linked ubiquitination on TRIM21 (**Figure 5M**).

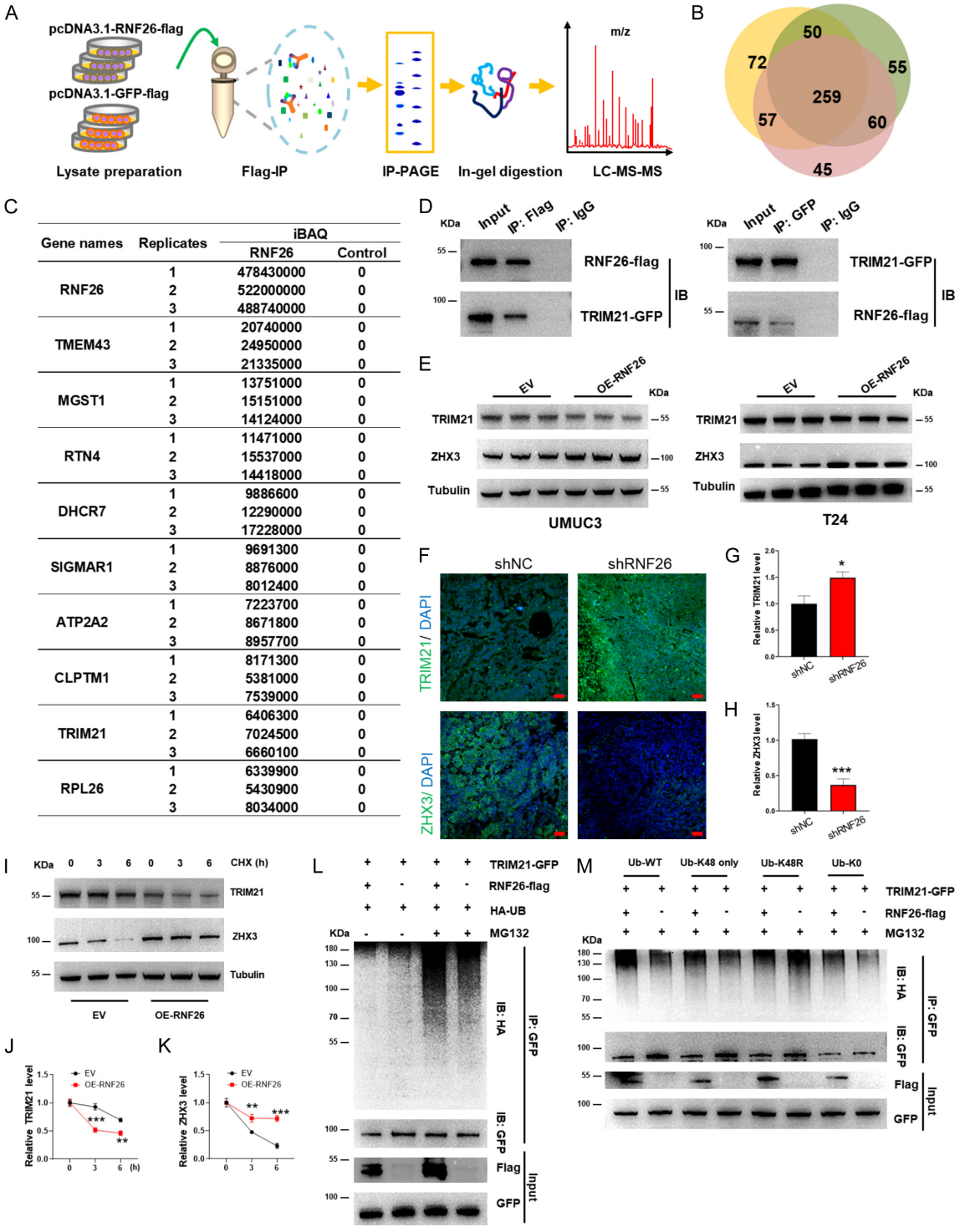


**Figure 5.** RNF26 interacts with TRIM21 in bladder cancer cells. A. The flowchart of immunoprecipitation-liquid chromatography tandem mass spectrometry (IP-LC-MS/MS) analyses in T24 cells. B. Venn diagram of three independent IP-LC-MS/MS assays of proteins. C. List of Top 10 proteins based on iBAQ quantification. D. The interaction between RNF26 and TRIM21 was confirmed by co-immunoprecipitation in T24 cells. E. RNF26 overexpressing in UMUC3 and T24 cells reduced TRIM21 protein expression and promotes ZHX3 expression. F-H. Immunostaining of xenograft tumor shows that TRIM21 expression was increased and ZHX3 expression was decreased with RNF26 knockdown. n = 3 for each group. Scale bar: 50 μm. I-K. Cycloheximide (CHX) treatment significantly shortened the half-life of TRIM21 protein and increased the half-life of ZHX3 protein after overexpression of RNF26 in T24 cells. L. Overexpression of RNF26 increased the level of polyubiquitination of TRIM21 in T24 cells. M. RNF26 promoted K48-linked ubiquitination on TRIM21 in T24 cells. *P < 0.05, **P < 0.01; ***P < 0.001.

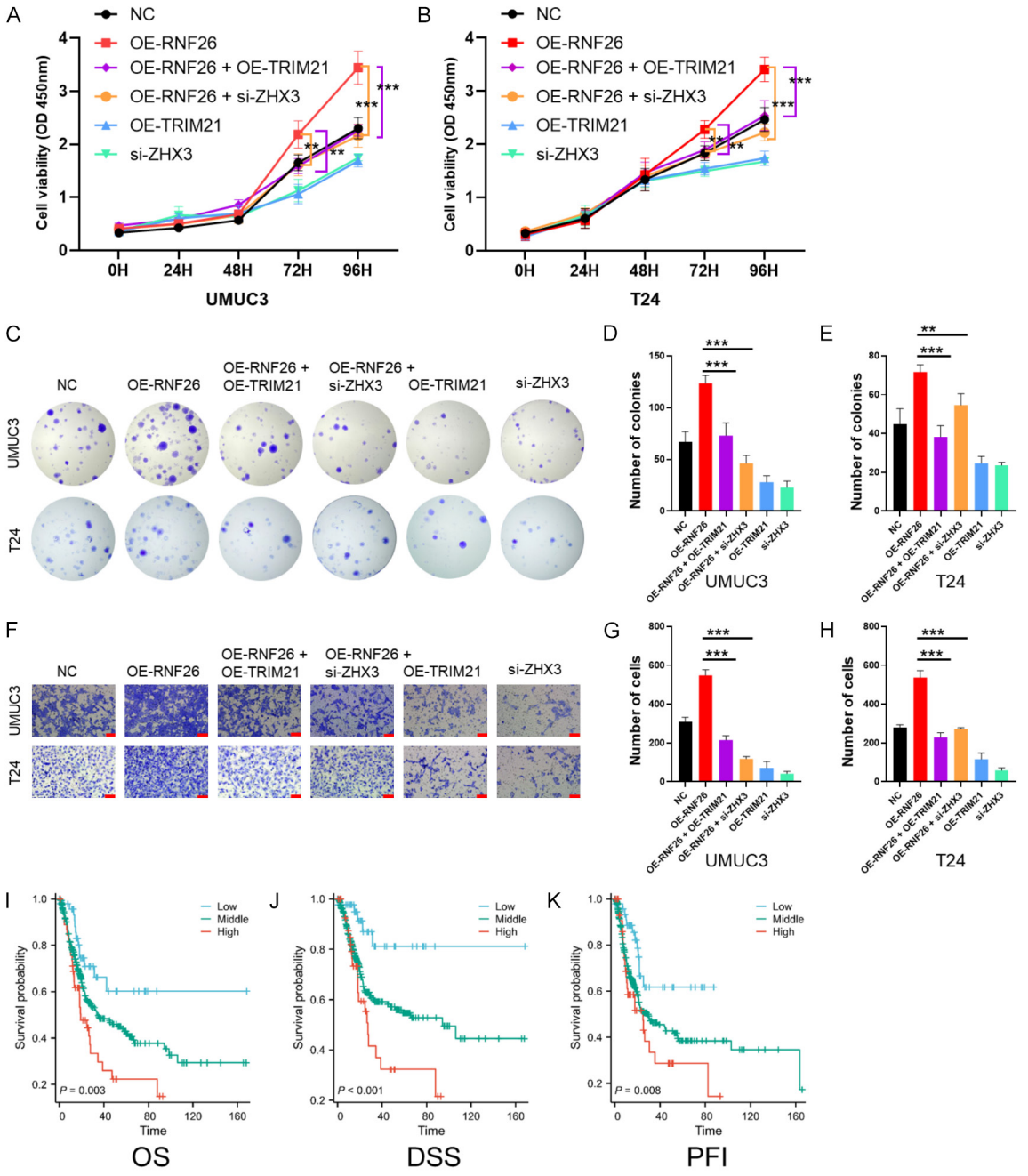


**Figure 6.** RNF26/TRIM21 induced bladder cancer cell proliferation and migration through ZHX3. TRIM21 overexpressing or ZHX3 silencing rescued the effects of RNF26 overexpressing on cell proliferation (A, B), migration (C-E), and colony formation (F-H) capacities of T24 and UMUC3 cells. (I-K) low risk group (low RNF26+high TRIM21+low ZHX3) were related to the good overall survival (OS) (I), disease specific survival(DSS) (J) and progress free interval (PFI) (K) in bladder cancer. Low risk group: low RNF26+high TRIM21+low ZHX3, high risk group: high RNF26+low TRIM21+high ZHX3, middle risk group: except for low RNF26+high TRIM21+low ZHX3 and high RNF26+low TRIM21+high ZHX3. Scale bar: 100 μm. *P < 0.05, **P < 0.01; ***P < 0.001.

*RNF26/TRIM21 induced bladder cancer cell proliferation and migration through ZHX3*

To further explore the functional association between RNF26 and TRIM21, rescue experiments were performed and analyzed. The results revealed a decrease in T24 and UMUC3 cell proliferation (**Figure 6A**, **6B**), migration (**Figure 6C-E**), and colony formation (**Figure 6F-H**) following the overexpression of TRIM21.

Simultaneously, TRIM21 overexpressing rescued the effects of RNF26 overexpressing on cell proliferation (**Figure 6A**, **6B**), migration (**Figure 6C-E**), and colony formation (**Figure 6F-H**) capacities of T24 and UMUC3 cells. Moreover, TRIM21 silencing rescued the effects of RNF26 silencing on cell proliferation (Figure S1A, S1B), migration (Figure S1C-E), and colony formation (Figure S1F-H) capacities of T24 and UMUC3 cells. To explore whether ZHX3 is a target molecule of RNF26/TRIM21 for their oncogenic function, cell rescue assays were also performed. As expected, ZHX3 silencing decreased T24 and UMUC3 cell proliferation (**Figure 6A**, **6B**), migration (**Figure 6C-E**), and colony formation (**Figure 6F-H**). Simultaneously, ZHX3 silencing reversed the effect of RNF26 overexpressing on cell proliferation (**Figure 6A**, **6B**), migration (**Figure 6C-E**), and colony formation (**Figure 6F-H**) capacities of T24 and UMUC3 cells. Moreover, ZHX3 overexpressing reversed the effect of RNF26 silencing on cell proliferation (Figure S1A, S1B), migration (Figure S1C-E), and colony formation (Figure S1F-H) capacities of T24 and UMUC3 cells.

Finally, we also validated the clinical significance of RNF26/TRIM21/ZHX3 axis in bladder cancer patients. KM survival analysis showed that patients with low risk group (low RNF26+ high TRIM21+low ZHX3) were related to the good overall survival (OS) (**Figure 6I**), disease free survival (DFS) (**Figure 6J**) and progress free interval (PFI) (**Figure 6K**) in bladder cancer. In contrast, patients with high risk (high RNF26+low TRIM21+high ZHX3) had the worst prognosis.

## Discussion

Bladder cancer is one of the prevalent urological malignancies, and existing therapeutic strategies including immunotherapy and immune checkpoint inhibitors are effective but with limitations in the treatment of bladder cancer patients [32]. New molecular mechanisms remain to be explored to improve the therapeutic outcome of bladder cancer. It has been demonstrated that E3 ubiquitin ligases are closely related to bladder carcinogenesis, metastasis, drug resistance and immune escape [33, 34]. RNF26, a key E3 ubiquitin ligase, has been reported to promote bladder cancer progression by regulating the cell cycle [15]. However, its role and related mechanisms in immune infiltration, immunotherapy, chemotherapeutic drug efficacy and tumor progression in bladder cancer remain to be elucidated. In this study, RNF26 expression was found to be closely associated with the efficacy of immunochemical drugs by biomimetic analysis, and Co-immunoprecipitation (Co-IP) assays and mass spectrometry (MS) analysis identified 259 potential RNF26 binding proteins. Among these, TRIM21 was an important binding protein of RNF26 and its ubiquitination was found mediated by RNF26 to affect its stability and to upregulate ZHX3, so as to influence bladder cancer progression.

Previous studies have demonstrated that RNF26 is upregulated in bladder cancer tissues and is strongly associated with poor prognosis [15]. Moreover, immune cell infiltration, such as macrophages, is strongly associated with tumor progression [35]. Corresponding to this, we have found in our study that low RNF26 expression displayed more immune cell infiltration, which may antagonize tumor cells, leading to better prognosis of bladder cancer. Meanwhile, immune checkpoint molecules were highly expressed in patients with high level RNF26, suggesting that such patients might be sensitive to immune checkpoint drugs. In addition, chemotherapy drug sensitivity analysis revealed that the RNF26 high expression group was more sensitive to cisplatin, VEGFR-targeted drugs and MET-targeted drugs. The fact that high level RNF26 expression (even with a poor prognosis), was sensitive to immune checkpoint drugs and multiple chemotherapeutic agents suggests that RNF26 may serve as a better predictive marker for the efficacy, and thus, better treatment strategy for bladder cancer.

To explore the effect of RNF26 in bladder cancer, functional assays were performed. A significant reduction in cell proliferation migration and colony-forming capacity was observed in the RNF26 knocking-down group compared to the control group. Meanwhile, overexpression of RNF26 in T24 and UMUC3 cells confirmed its oncogenic function. Xenograft assays further confirmed that knockdown of RNF26 resulted in reduced tumor growth. Previous studies have suggested that RNF26 binds to p57 and affects its stability through ubiquitination which is involved in the aggressiveness of bladder cancer [15]. Moreover, this study iden-

tified many other candidate proteins that may bind to RNF26 to influence its function. Indeed, 259 potential RNF26 binding proteins were identified by mass spectrometry analysis in this study. Interestingly, among the 259 identified proteins, TRIM21, an RNF26-binding protein with an E3 ubiquitin ligase active RING domain at its N-terminal end, could degrade different proteins by ubiquitination [36]. TRIM21 has been shown to have oncogenic effects on a variety of tumors through the ubiquitination pathway. For example, TRIM21 increases the ubiquitination and degradation of octamer-binding transcription factor 1 (Oct-1), which is self-renewed by cancer stem cells, resulting in stem cell reduction [37]. The cell cycle protein-dependent kinase 2 (CDK2) complex is hyperactivated in most cancers [38, 39], and TRIM21 can promote CDK2 autophagic degradation, thereby inhibiting leukemia progression [40]. All these suggest that RNF26 may promote bladder cancer progression by inhibiting TRIM21 function. Indeed, Co-IP experiments, Cycloheximide (CHX) treatment and ubiquitination assays, confirmed that RNF26 exerts an oncogenic function by binding to TRIM21 and promoting its ubiquitination. In addition, it has been reported that ZHX3 is an important target molecule of TRIM21 in bladder cancer and is closely associated with bladder cancer invasion, migration and poor prognosis. To clarify whether ZHX3 is the downstream target of RNF26/TRIM21. Rescue experiments were performed and the results showed that ZHX3 silencing reversed the effects of RNF26 overexpression on the proliferation, migration and colony-forming ability of bladder cancer cells. In addition, the RNF26/TRIM21/ZHX3 axis was also confirmed to be closely associated with poor prognosis of bladder cancer patients.

In summary, our study provides evidence that RNF26 is closely associated with poor prognosis, chemotherapeutic drug efficacy and immune checkpoint blockade therapy benefits of bladder cancer. RNF26 may bind to TRIM21 to regulate its protein stability and play an oncogenic role in bladder cancer through ZHX3. Together, these data support that RNF26 is a potential efficacy predictive marker and a therapeutic target for patients with bladder cancer.

## Acknowledgements

We would like to thank Walgenron Bio-Pharm Co., Ltd (Shenzhen, China) for language editing. This study was supported by the project of Jiangsu Province Traditional Chinese Medicine Technology Development (MS2022100).

## Disclosure of conflict of interest

None.

**Address correspondence to:** Xiaozhou He, Department of Urology, The Third Affiliated Hospital of Soochow University, Soochow University, No. 185, Juqian Street, Changzhou 213000, Jiangsu, China. Tel: +86-13901507500; E-mail: xiaozhouhe123@163.com; hyx@suda.edu.cn

## References

[1] Sung H, Ferlay J, Siegel RL, Laversanne M, Soerjomataram I, Jemal A and Bray F. Global cancer statistics 2020: GLOBOCAN estimates of incidence and mortality worldwide for 36 cancers in 185 countries. CA Cancer J Clin 2021; 71: 209-249.

[2] Han X, Zhang T, Ma Q, Chang R, Xin S, Yu Q, Zhang G and Wang Y. Gene expression profiles to analyze the anticancer and carcinogenic effects of arsenic in bladder cancer. Am J Transl Res 2023; 15: 5984-5996.

[3] Lenis AT, Lec PM, Chamie K and Mshs MD. Bladder cancer: a review. JAMA 2020; 324: 1980-1991.

[4] Tan WS, Steinberg G, Witjes JA, Li R, Shariat SF, Roupret M, Babjuk M, Bivalacqua TJ, Psutka SP, Williams SB, Cookson MS, Palou J and Kamat AM. Intermediate-risk non-muscle-invasive bladder cancer: updated consensus definition and management recommendations from the international bladder cancer group. Eur Urol Oncol 2022; 5: 505-516.

[5] Cai H, Chen H, Huang Q, Zhu JM, Ke ZB, Lin YZ, Zheng QS, Wei Y, Xu N and Xue XY. Ubiquitination-related molecular subtypes and a novel prognostic index for bladder cancer patients. Pathol Oncol Res 2021; 27: 1609941.

[6] Squair DR and Virdee S. A new dawn beyond lysine ubiquitination. Nat Chem Biol 2022; 18: 802-811.

[7] Li H, Yang F, Chang K, Yu X, Guan F and Li X. The synergistic function of long and short forms of β4GalT1 in p53-mediated drug resistance in bladder cancer cells. Biochim Biophys Acta Mol Cell Res 2023; 1870: 119409.

[8] Chen C and Matesic LE. The Nedd4-like family of E3 ubiquitin ligases and cancer. Cancer Metastasis Rev 2007; 26: 587-604.

[9] Jongsma ML, Berlin I, Wijdeven RH, Janssen L, Janssen GM, Garstka MA, Janssen H, Mensink M, van Veelen PA, Spaapen RM and Neefjes J.

An ER-associated pathway defines endosomal architecture for controlled cargo transport. Cell 2016; 166: 152-166.
[10] Cremer T, Jongsma MLM, Trulsson F, Vertegaal ACO, Neefjes J and Berlin I. The ER-embedded UBE2J1/RNF26 ubiquitylation complex exerts spatiotemporal control over the endolysosomal pathway. Cell Rep 2021; 34: 108659.
[11] Cremer T, Voortman LM, Bos E, Jongsma ML, Ter Haar LR, Akkermans JJ, Talavera Ormeno CM, Wijdeven RH, de Vries J, Kim RQ, Janssen GM, van Veelen PA, Koning RI, Neefjes J and Berlin I. RNF26 binds perinuclear vimentin filaments to integrate ER and endolysosomal responses to proteotoxic stress. EMBO J 2023; 42: e111252.
[12] Katoh M. Molecular cloning and characterization of RNF26 on human chromosome 11q23 region, encoding a novel RING finger protein with leucine zipper. Biochem Biophys Res Commun 2001; 282: 1038-1044.
[13] Lu X, Zhang Y, Wu Y, Lu T, Yang H, Yang W, Pang B and Yang C. RNF26 promotes pancreatic cancer proliferation by enhancing RBM38 degradation. Pancreas 2022; 51: 1427-1433.
[14] Liu W, Wang H, Jian C, Li W, Ye K, Ren J, Zhu L, Wang Y, Jin X and Yi L. The RNF26/CBX7 axis modulates the TNF pathway to promote cell proliferation and regulate sensitivity to TKIs in ccRCC. Int J Biol Sci 2022; 18: 2132-2145.
[15] Yi L, Wang H, Li W, Ye K, Xiong W, Yu H and Jin X. The FOXM1/RNF26/p57 axis regulates the cell cycle to promote the aggressiveness of bladder cancer. Cell Death Dis 2021; 12: 944.
[16] Newman AM, Steen CB, Liu CL, Gentles AJ, Chaudhuri AA, Scherer F, Khodadoust MS, Esfahani MS, Luca BA, Steiner D, Diehn M and Alizadeh AA. Determining cell type abundance and expression from bulk tissues with digital cytometry. Nat Biotechnol 2019; 37: 773-782.
[17] Feng B, Zhou T, Guo Z, Jin J, Zhang S, Qiu J, Cao J, Li J, Peng X, Wang J, Xing Y, Ji R, Qiao L and Liang Y. Comprehensive analysis of immune-related genes for classification and immune microenvironment of asthma. Am J Transl Res 2023; 15: 1052-1062.
[18] Wang X, Xu Y, Dai L, Yu Z, Wang M, Chan S, Sun R, Han Q, Chen J, Zuo X, Wang Z, Hu X, Yang Y, Zhao H, Hu K, Zhang H and Chen W. A novel oxidative stress- and ferroptosis-related gene prognostic signature for distinguishing cold and hot tumors in colorectal cancer. Front Immunol 2022; 13: 1043738.
[19] Xuan J, Li F, Li J, Gong C, Li J, Mo Z and Jin Q. The role of senescence genes in the treatment, prognosis, and tumor microenvironment of gastric cancer. Am J Transl Res 2023; 15: 6926-6938.
[20] Geeleher P, Cox N and Huang RS. pRRophetic: an R package for prediction of clinical chemotherapeutic response from tumor gene expression levels. PLoS One 2014; 9: e107468.
[21] Zhang K, Xu J, Ding Y, Shen C, Lin M, Dai X, Zhou H, Huang X, Xue B and Zheng B. BMI1 promotes spermatogonia proliferation through epigenetic repression of Ptprm. Biochem Biophys Res Commun 2021; 583: 169-177.
[22] Wang Q, Wu Y, Lin M, Wang G, Liu J, Xie M, Zheng B, Shen C and Shen J. BMI1 promotes osteosarcoma proliferation and metastasis by repressing the transcription of SIK1. Cancer Cell Int 2022; 22: 136.
[23] Zhou J, Li J, Qian C, Qiu F, Shen Q, Tong R, Yang Q, Xu J, Zheng B, Lv J and Hou J. LINC00624/TEX10/NF-κB axis promotes proliferation and migration of human prostate cancer cells. Biochem Biophys Res Commun 2022; 601: 1-8.
[24] Wang J, Zhao J, Lin L, Peng X, Li W, Huang Y, Wang K and Li J. LncRNA-Anrel promotes the proliferation and migration of synovial fibroblasts through regulating miR-146a-mediated annexin A1 expression. Am J Clin Exp Immunol 2023; 12: 49-59.
[25] Xu W, Wang J, Xu J, Li S, Zhang R, Shen C, Xie M, Zheng B and Gu M. Long non-coding RNA DEPDC1-AS1 promotes proliferation and migration of human gastric cancer cells HGC-27 via the human antigen R-F11R pathway. J Int Med Res 2022; 50: 3000605221093135.
[26] Chen X, Zheng Y, Han Y, He H, Lv J, Yu J, Li H, Hou S, Shen C and Zheng B. SAT2 regulates Sertoli cell-germline interactions via STIM1-mediated ROS/WNT/β-catenin signaling pathway. Cell Biol Int 2022; 46: 1704-1713.
[27] Wu Y, Shen C, Wu T, Huang X, Li H and Zheng B. Syntaxin binding protein 2 in sertoli cells regulates spermatogonial stem cell maintenance through directly interacting with connexin 43 in the testes of neonatal mice. Mol Biol Rep 2022; 49: 7557-7566.
[28] Xue J, Wu T, Huang C, Shu M, Shen C, Zheng B and Lv J. Identification of proline-rich protein 11 as a major regulator in mouse spermatogonia maintenance via an increase in BMI1 protein stability. Mol Biol Rep 2022; 49: 9555-9564.
[29] Skejoe C, Hansen AS, Stengaard-Pedersen K, Junker P, Hoerslev-Pedersen K, Hetland ML, Oestergaard M, Greisen S, Hvid M, Deleuran M and Deleuran B. T-cell immunoglobulin and mucin domain 3 is upregulated in rheumatoid arthritis, but insufficient in controlling inflammation. Am J Clin Exp Immunol 2022; 11: 34-44.
[30] Deng M, Wei W, Duan J, Chen R, Wang N, He L, Peng Y, Ma X, Wu Z, Liu J, Li Z, Zhang Z, Jiang L, Zhou F and Xie D. ZHX3 promotes the progres-

sion of urothelial carcinoma of the bladder via repressing of RGS2 and is a novel substrate of TRIM21. Cancer Sci 2021; 112: 1758-1771.
[31] Wang L, Zhang X, Lin ZB, Yang PJ, Xu H, Duan JL, Ruan B, Song P, Liu JJ, Yue ZS, Fang ZQ, Hu H, Liu Z, Huang XL, Yang L, Tian S, Tao KS, Han H and Dou KF. Tripartite motif 16 ameliorates nonalcoholic steatohepatitis by promoting the degradation of phospho-TAK1. Cell Metab 2021; 33: 1372-1388, e1377.
[32] Saidian A, Dolendo I, Sharabi A, Stewart TF, Rose B, McKay RR, Bagrodia A and Salmasi A. The current and future promises of combination radiation and immunotherapy for genitourinary cancers. Cancers (Basel) 2022; 15: 127.
[33] Wang X, Zhang Y, Wu Y, Cheng H and Wang X. The role of E3 ubiquitin ligases and deubiquitinases in bladder cancer development and immunotherapy. Front Immunol 2023; 14: 1202633.
[34] Iyengar PV, Marvin DL, Lama D, Tan TZ, Suriyamurthy S, Xie F, van Dinther M, Mei H, Verma CS, Zhang L, Ritsma L and Ten Dijke P. TRAF4 inhibits bladder cancer progression by promoting BMP/SMAD signaling. Mol Cancer Res 2022; 20: 1516-1531.
[35] Zhu J, Wang H, Ma T, He Y, Shen M, Song W, Wang JJ, Shi JP, Wu MY, Liu C, Wang WJ and Huang YQ. Identification of immune-related genes as prognostic factors in bladder cancer. Sci Rep 2020; 10: 19695.
[36] Chen X, Cao M, Wang P, Chu S, Li M, Hou P, Zheng J, Li Z and Bai J. The emerging roles of TRIM21 in coordinating cancer metabolism, immunity and cancer treatment. Front Immunol 2022; 13: 968755.
[37] Du L, Li YJ, Fakih M, Wiatrek RL, Duldulao M, Chen Z, Chu P, Garcia-Aguilar J and Chen Y. Role of SUMO activating enzyme in cancer stem cell maintenance and self-renewal. Nat Commun 2016; 7: 12326.
[38] Huang H, Regan KM, Lou Z, Chen J and Tindall DJ. CDK2-dependent phosphorylation of FOXO1 as an apoptotic response to DNA damage. Science 2006; 314: 294-297.
[39] Volkart PA, Bitencourt-Ferreira G, Souto AA and de Azevedo WF. Cyclin-dependent kinase 2 in cellular senescence and cancer. A structural and functional review. Curr Drug Targets 2019; 20: 716-726.
[40] Zhang J, Gan Y, Li H, Yin J, He X, Lin L, Xu S, Fang Z, Kim BW, Gao L, Ding L, Zhang E, Ma X, Li J, Li L, Xu Y, Horne D, Xu R, Yu H, Gu Y and Huang W. Inhibition of the CDK2 and cyclin a complex leads to autophagic degradation of CDK2 in cancer cells. Nat Commun 2022; 13: 2835.

**Table S1.** Putative interactors identified from three independent experiments in this study

| Gene names | Unique peptides control_rep1 | Unique peptides control_rep2 | Unique peptides control_rep3 | Unique peptides RNF26_rep1 | Unique peptides RNF26_rep2 | Unique peptides RNF26_rep3 | iBAQ control_ rep1 | iBAQ control_ rep2 | iBAQ control_ rep3 | iBAQ RNF26_rep1 | iBAQ RNF26_rep2 | iBAQ RNF26_rep3 |
|---|---|---|---|---|---|---|---|---|---|---|---|---|
| RNF26 | 0 | 0 | 0 | 21 | 18 | 18 | 0 | 0 | 0 | 478430000 | 522000000 | 488740000 |
| TMEM43 | 0 | 0 | 0 | 17 | 22 | 19 | 0 | 0 | 0 | 20740000 | 24950000 | 21335000 |
| MGST1 | 0 | 0 | 0 | 4 | 4 | 4 | 0 | 0 | 0 | 13751000 | 15151000 | 14124000 |
| RTN4 | 0 | 0 | 0 | 6 | 9 | 7 | 0 | 0 | 0 | 11471000 | 15537000 | 14418000 |
| DHCR7 | 0 | 0 | 0 | 4 | 5 | 8 | 0 | 0 | 0 | 9886600 | 12290000 | 17228000 |
| SIGMAR1 | 0 | 0 | 0 | 3 | 3 | 3 | 0 | 0 | 0 | 9691300 | 8876000 | 8012400 |
| ATP2A2 | 0 | 0 | 0 | 23 | 32 | 27 | 0 | 0 | 0 | 7223700 | 8671800 | 8957700 |
| CLPTM1 | 0 | 0 | 0 | 14 | 13 | 15 | 0 | 0 | 0 | 8171300 | 5381000 | 7539000 |
| TRIM21 | 0 | 0 | 0 | 15 | 18 | 14 | 0 | 0 | 0 | 6406300 | 7024500 | 6660100 |
| RPL26 | 0 | 0 | 0 | 4 | 4 | 6 | 0 | 0 | 0 | 6339900 | 5430900 | 8034000 |
| RPL27A | 0 | 0 | 0 | 4 | 5 | 4 | 0 | 0 | 0 | 6133000 | 6617300 | 6483400 |
| RPL23 | 0 | 0 | 0 | 3 | 2 | 4 | 0 | 0 | 0 | 4335700 | 6096900 | 8473600 |
| LGALS3BP | 0 | 0 | 0 | 10 | 13 | 12 | 0 | 0 | 0 | 4383000 | 5316700 | 4814500 |
| RPS13 | 0 | 0 | 0 | 7 | 5 | 5 | 0 | 0 | 0 | 4894600 | 4284400 | 4334100 |
| GNB2 | 0 | 0 | 0 | 3 | 4 | 3 | 0 | 0 | 0 | 2087800 | 3353000 | 6767900 |
| EMC4 | 0 | 0 | 0 | 4 | 4 | 3 | 0 | 0 | 0 | 4331300 | 3104300 | 2971500 |
| BCAP31 | 0 | 0 | 0 | 6 | 8 | 8 | 0 | 0 | 0 | 2853700 | 3213200 | 4171400 |
| RER1 | 0 | 0 | 0 | 2 | 2 | 4 | 0 | 0 | 0 | 3145400 | 3120900 | 3800400 |
| SPCS3 | 0 | 0 | 0 | 3 | 3 | 2 | 0 | 0 | 0 | 3904800 | 3205600 | 1872700 |
| HACD3 | 0 | 0 | 0 | 5 | 9 | 7 | 0 | 0 | 0 | 2513400 | 3266800 | 3118600 |
| DHCR24 | 0 | 0 | 0 | 7 | 8 | 8 | 0 | 0 | 0 | 2966600 | 2769000 | 3036800 |
| CAV2 | 0 | 0 | 0 | 3 | 3 | 2 | 0 | 0 | 0 | 2025300 | 3486600 | 3153400 |
| SLC25A11 | 0 | 0 | 0 | 7 | 8 | 7 | 0 | 0 | 0 | 3266000 | 2766800 | 2608200 |
| RPL34 | 0 | 0 | 0 | 3 | 3 | 4 | 0 | 0 | 0 | 1718100 | 1730400 | 4647500 |
| CPT1A | 0 | 0 | 0 | 13 | 11 | 12 | 0 | 0 | 0 | 2729900 | 2231400 | 2830800 |
| TMED10 | 0 | 0 | 0 | 3 | 3 | 3 | 0 | 0 | 0 | 2559000 | 2436800 | 2785400 |
| EBP | 0 | 0 | 0 | 2 | 2 | 2 | 0 | 0 | 0 | 2534700 | 2183000 | 2878400 |
| RPL5 | 0 | 0 | 0 | 5 | 6 | 4 | 0 | 0 | 0 | 2579100 | 2644000 | 2247200 |
| RPL35A | 0 | 0 | 0 | 4 | 2 | 3 | 0 | 0 | 0 | 2976100 | 1636500 | 2720700 |
| COPA | 0 | 0 | 0 | 23 | 29 | 26 | 0 | 0 | 0 | 2224500 | 2498200 | 2565900 |
| SEC62 | 0 | 0 | 0 | 2 | 2 | 3 | 0 | 0 | 0 | 1294700 | 2506300 | 3475800 |
| UQCR10 | 0 | 0 | 0 | 2 | 2 | 2 | 0 | 0 | 0 | 2022600 | 2573000 | 2203100 |
| ATP5F1 | 0 | 0 | 0 | 4 | 4 | 7 | 0 | 0 | 0 | 1662100 | 2161700 | 2914000 |
| OPA1 | 0 | 0 | 0 | 23 | 24 | 18 | 0 | 0 | 0 | 2343100 | 2413600 | 1966300 |
| ERLIN2 | 0 | 0 | 0 | 4 | 5 | 5 | 0 | 0 | 0 | 2049800 | 1940300 | 2618200 |
| MYO1C | 0 | 0 | 0 | 14 | 19 | 19 | 0 | 0 | 0 | 1528900 | 2369400 | 2493200 |

| | | | | | | | | | | | |
|---|---|---|---|---|---|---|---|---|---|---|---|
| RPL10A | 0 | 0 | 0 | 4 | 5 | 4 | 0 | 0 | 0 | 1753400 | 2379900 | 2233100 |
| CRMP1 | 0 | 0 | 0 | 5 | 4 | 3 | 0 | 0 | 0 | 418070 | 2807800 | 3119400 |
| FITM2 | 0 | 0 | 0 | 3 | 3 | 3 | 0 | 0 | 0 | 2126400 | 1875500 | 2070300 |
| SNX2 | 0 | 0 | 0 | 10 | 11 | 10 | 0 | 0 | 0 | 1598700 | 2103600 | 1896500 |
| TAP1 | 0 | 0 | 0 | 9 | 8 | 9 | 0 | 0 | 0 | 1991800 | 1562000 | 1957000 |
| PFN2 | 0 | 0 | 0 | 3 | 2 | 3 | 0 | 0 | 0 | 2497000 | 887140 | 2117800 |
| CANX | 0 | 0 | 0 | 7 | 10 | 10 | 0 | 0 | 0 | 1382200 | 1964400 | 2047700 |
| RPS18 | 0 | 0 | 0 | 4 | 6 | 4 | 0 | 0 | 0 | 1407600 | 2685200 | 754050 |
| SLC25A1 | 0 | 0 | 0 | 5 | 3 | 5 | 0 | 0 | 0 | 1877200 | 956210 | 1770900 |
| NUP205 | 0 | 0 | 0 | 34 | 30 | 33 | 0 | 0 | 0 | 1522300 | 1537700 | 1493200 |
| PRKDC | 0 | 0 | 0 | 50 | 58 | 61 | 0 | 0 | 0 | 1220800 | 1515600 | 1703200 |
| EMC3 | 0 | 0 | 0 | 2 | 5 | 4 | 0 | 0 | 0 | 851920 | 1941400 | 1619300 |
| THEM6 | 0 | 0 | 0 | 4 | 6 | 5 | 0 | 0 | 0 | 1214900 | 1602500 | 1495100 |
| CYFIP1 | 0 | 0 | 0 | 12 | 14 | 16 | 0 | 0 | 0 | 1405200 | 1449600 | 1404400 |
| TAP2 | 0 | 0 | 0 | 7 | 5 | 6 | 0 | 0 | 0 | 1735700 | 953240 | 1534100 |
| CLN6 | 0 | 0 | 0 | 2 | 2 | 2 | 0 | 0 | 0 | 1520700 | 1366900 | 1331200 |
| LBR | 0 | 0 | 0 | 5 | 4 | 4 | 0 | 0 | 0 | 1437200 | 1284900 | 1476600 |
| FDPS | 0 | 0 | 0 | 5 | 5 | 5 | 0 | 0 | 0 | 1047600 | 1413100 | 1732300 |
| ATL3 | 0 | 0 | 0 | 4 | 6 | 7 | 0 | 0 | 0 | 1080000 | 1354000 | 1750600 |
| WARS | 0 | 0 | 0 | 8 | 10 | 8 | 0 | 0 | 0 | 1372600 | 1444400 | 1195600 |
| VARS | 0 | 0 | 0 | 18 | 15 | 18 | 0 | 0 | 0 | 1397100 | 1194500 | 1359000 |
| C14orf1 | 0 | 0 | 0 | 2 | 3 | 2 | 0 | 0 | 0 | 1305200 | 1127300 | 1371700 |
| DHX9 | 0 | 0 | 0 | 16 | 15 | 14 | 0 | 0 | 0 | 1258000 | 1250500 | 1255500 |
| PLIN3 | 0 | 0 | 0 | 5 | 7 | 6 | 0 | 0 | 0 | 1117100 | 1319700 | 1244800 |
| CTPS1 | 0 | 0 | 0 | 10 | 9 | 9 | 0 | 0 | 0 | 1032800 | 1259400 | 1251900 |
| TMEM159 | 0 | 0 | 0 | 2 | 2 | 2 | 0 | 0 | 0 | 1196600 | 1018600 | 1091300 |
| XPO1 | 0 | 0 | 0 | 9 | 13 | 14 | 0 | 0 | 0 | 832640 | 1097400 | 1230400 |
| ACOT9 | 0 | 0 | 0 | 5 | 6 | 5 | 0 | 0 | 0 | 1199800 | 1037000 | 885010 |
| JAGN1 | 0 | 0 | 0 | 2 | 2 | 2 | 0 | 0 | 0 | 1047900 | 1016200 | 1052500 |
| LPCAT1 | 0 | 0 | 0 | 6 | 5 | 4 | 0 | 0 | 0 | 1259000 | 1064500 | 762700 |
| HSD17B12 | 0 | 0 | 0 | 2 | 5 | 4 | 0 | 0 | 0 | 1150900 | 905200 | 1021900 |
| PRPF19 | 0 | 0 | 0 | 4 | 4 | 4 | 0 | 0 | 0 | 858810 | 1082200 | 1132200 |
| EIF3E | 0 | 0 | 0 | 7 | 6 | 8 | 0 | 0 | 0 | 1095500 | 1154700 | 801100 |
| EMC2 | 0 | 0 | 0 | 3 | 3 | 3 | 0 | 0 | 0 | 1037700 | 1068200 | 939180 |
| SGPL1 | 0 | 0 | 0 | 5 | 5 | 4 | 0 | 0 | 0 | 993770 | 1071500 | 941570 |
| TRIP13 | 0 | 0 | 0 | 8 | 7 | 8 | 0 | 0 | 0 | 910340 | 858530 | 1025400 |
| NCLN | 0 | 0 | 0 | 8 | 6 | 8 | 0 | 0 | 0 | 1109400 | 611550 | 1071400 |
| EMD | 0 | 0 | 0 | 4 | 3 | 3 | 0 | 0 | 0 | 1010300 | 863970 | 883520 |
| TOMM22 | 0 | 0 | 0 | 2 | 2 | 3 | 0 | 0 | 0 | 507430 | 780060 | 1469000 |
| HSDL1 | 0 | 0 | 0 | 2 | 3 | 4 | 0 | 0 | 0 | 852110 | 858130 | 1037800 |

| | | | | | | | | | | | |
|---|---|---|---|---|---|---|---|---|---|---|---|
| COPE | 0 | 0 | 0 | 3 | 5 | 5 | 0 | 0 | 0 | 553640 | 944030 | 1171000 |
| SF3B1 | 0 | 0 | 0 | 10 | 13 | 12 | 0 | 0 | 0 | 597790 | 1037300 | 1008400 |
| PDCD6IP | 0 | 0 | 0 | 12 | 13 | 17 | 0 | 0 | 0 | 708450 | 756450 | 1149200 |
| ACTR2 | 0 | 0 | 0 | 4 | 2 | 3 | 0 | 0 | 0 | 840660 | 869490 | 897760 |
| ACTR3 | 0 | 0 | 0 | 4 | 4 | 3 | 0 | 0 | 0 | 997810 | 884970 | 719700 |
| HNRNPA0 | 0 | 0 | 0 | 3 | 4 | 5 | 0 | 0 | 0 | 747550 | 855420 | 995730 |
| MBOAT7 | 0 | 0 | 0 | 3 | 4 | 3 | 0 | 0 | 0 | 817470 | 908240 | 837080 |
| PSMA7 | 0 | 0 | 0 | 2 | 3 | 3 | 0 | 0 | 0 | 587600 | 938510 | 1020200 |
| AP2M1 | 0 | 0 | 0 | 5 | 7 | 4 | 0 | 0 | 0 | 942230 | 1102400 | 495020 |
| DYNC1H1 | 0 | 0 | 0 | 52 | 54 | 51 | 0 | 0 | 0 | 815640 | 859830 | 831370 |
| NDUFA9 | 0 | 0 | 0 | 5 | 9 | 7 | 0 | 0 | 0 | 575810 | 1019300 | 876790 |
| RAE1 | 0 | 0 | 0 | 3 | 4 | 2 | 0 | 0 | 0 | 693470 | 1031700 | 687790 |
| TEX10 | 0 | 0 | 0 | 9 | 9 | 8 | 0 | 0 | 0 | 902340 | 805340 | 654810 |
| OAS3 | 0 | 0 | 0 | 11 | 10 | 12 | 0 | 0 | 0 | 812430 | 697720 | 843100 |
| SEC22B | 0 | 0 | 0 | 5 | 3 | 3 | 0 | 0 | 0 | 1050200 | 546840 | 685860 |
| WDR1 | 0 | 0 | 0 | 5 | 5 | 4 | 0 | 0 | 0 | 764090 | 800450 | 710550 |
| IQGAP1 | 0 | 0 | 0 | 19 | 21 | 19 | 0 | 0 | 0 | 707010 | 757530 | 777310 |
| EIF2S2 | 0 | 0 | 0 | 3 | 4 | 5 | 0 | 0 | 0 | 644130 | 722550 | 838920 |
| SMPD4 | 0 | 0 | 0 | 5 | 6 | 5 | 0 | 0 | 0 | 883280 | 774160 | 546570 |
| NAMPT | 0 | 0 | 0 | 3 | 8 | 7 | 0 | 0 | 0 | 281500 | 1002100 | 875770 |
| LMAN1 | 0 | 0 | 0 | 3 | 3 | 3 | 0 | 0 | 0 | 474110 | 869760 | 782230 |
| PSMD6 | 0 | 0 | 0 | 7 | 7 | 6 | 0 | 0 | 0 | 860590 | 621990 | 620830 |
| CYP51A1 | 0 | 0 | 0 | 5 | 8 | 6 | 0 | 0 | 0 | 595900 | 928740 | 550390 |
| DNM1L | 0 | 0 | 0 | 9 | 10 | 7 | 0 | 0 | 0 | 616000 | 825320 | 612340 |
| VDAC1 | 0 | 0 | 0 | 4 | 5 | 4 | 0 | 0 | 0 | 618470 | 659710 | 760390 |
| Septin-7 | 0 | 0 | 0 | 5 | 5 | 5 | 0 | 0 | 0 | 692230 | 640610 | 677020 |
| BLVRA | 0 | 0 | 0 | 3 | 4 | 4 | 0 | 0 | 0 | 569980 | 621380 | 774360 |
| MRPS22 | 0 | 0 | 0 | 3 | 6 | 7 | 0 | 0 | 0 | 371550 | 683450 | 910650 |
| FBL | 0 | 0 | 0 | 2 | 2 | 3 | 0 | 0 | 0 | 373160 | 881420 | 709430 |
| RBM14 | 0 | 0 | 0 | 4 | 6 | 6 | 0 | 0 | 0 | 611220 | 703000 | 640480 |
| EEF1E1 | 0 | 0 | 0 | 2 | 2 | 2 | 0 | 0 | 0 | 611760 | 616420 | 724870 |
| TUBG1 | 0 | 0 | 0 | 2 | 3 | 2 | 0 | 0 | 0 | 429760 | 1034000 | 470130 |
| PDHB | 0 | 0 | 0 | 3 | 5 | 2 | 0 | 0 | 0 | 935860 | 733440 | 251240 |
| AIMP2 | 0 | 0 | 0 | 2 | 4 | 4 | 0 | 0 | 0 | 451080 | 710360 | 739450 |
| PIGT | 0 | 0 | 0 | 6 | 5 | 3 | 0 | 0 | 0 | 652620 | 708640 | 524850 |
| TMEM194A | 0 | 0 | 0 | 3 | 3 | 3 | 0 | 0 | 0 | 463980 | 720970 | 694390 |
| NOP56 | 0 | 0 | 0 | 7 | 7 | 6 | 0 | 0 | 0 | 570160 | 701910 | 581110 |
| DLD | 0 | 0 | 0 | 4 | 5 | 6 | 0 | 0 | 0 | 638280 | 615690 | 595430 |
| PEX11B | 0 | 0 | 0 | 4 | 4 | 3 | 0 | 0 | 0 | 501940 | 655090 | 688970 |
| EIF3B | 0 | 0 | 0 | 7 | 6 | 10 | 0 | 0 | 0 | 571680 | 548370 | 695080 |

| | | | | | | | | | | | |
|---|---|---|---|---|---|---|---|---|---|---|---|
| ADSL | 0 | 0 | 0 | 4 | 2 | 3 | 0 | 0 | 0 | 693210 | 476700 | 645180 |
| GTPBP4 | 0 | 0 | 0 | 7 | 6 | 5 | 0 | 0 | 0 | 765830 | 621990 | 406700 |
| Septin-2 | 0 | 0 | 0 | 3 | 5 | 4 | 0 | 0 | 0 | 412350 | 786150 | 590010 |
| SF3B6 | 0 | 0 | 0 | 2 | 3 | 3 | 0 | 0 | 0 | 224820 | 832720 | 726030 |
| EIF3A | 0 | 0 | 0 | 9 | 7 | 9 | 0 | 0 | 0 | 616940 | 527760 | 613210 |
| PIGK | 0 | 0 | 0 | 4 | 3 | 4 | 0 | 0 | 0 | 741000 | 412740 | 592530 |
| ARCN1 | 0 | 0 | 0 | 7 | 8 | 4 | 0 | 0 | 0 | 689760 | 589260 | 449010 |
| P4HA1 | 0 | 0 | 0 | 5 | 5 | 5 | 0 | 0 | 0 | 615940 | 522520 | 573990 |
| HSD17B11 | 0 | 0 | 0 | 3 | 3 | 2 | 0 | 0 | 0 | 572330 | 614420 | 524310 |
| MYO1B | 0 | 0 | 0 | 8 | 11 | 11 | 0 | 0 | 0 | 461220 | 640090 | 579850 |
| VPS26A | 0 | 0 | 0 | 3 | 2 | 2 | 0 | 0 | 0 | 705550 | 457670 | 513190 |
| ACTR1A | 0 | 0 | 0 | 2 | 4 | 4 | 0 | 0 | 0 | 219470 | 743520 | 704980 |
| PSMC2 | 0 | 0 | 0 | 6 | 7 | 5 | 0 | 0 | 0 | 541160 | 595430 | 528210 |
| PTRF | 0 | 0 | 0 | 2 | 2 | 2 | 0 | 0 | 0 | 456120 | 572100 | 594380 |
| ARPC2 | 0 | 0 | 0 | 4 | 4 | 4 | 0 | 0 | 0 | 549710 | 550970 | 519960 |
| NUP93 | 0 | 0 | 0 | 7 | 8 | 9 | 0 | 0 | 0 | 438270 | 467010 | 709900 |
| MAT2B | 0 | 0 | 0 | 2 | 2 | 2 | 0 | 0 | 0 | 514970 | 544690 | 504020 |
| UBAC2 | 0 | 0 | 0 | 3 | 2 | 4 | 0 | 0 | 0 | 508130 | 399460 | 636060 |
| SYVN1 | 0 | 0 | 0 | 2 | 2 | 2 | 0 | 0 | 0 | 523610 | 571520 | 446200 |
| ABCD3 | 0 | 0 | 0 | 6 | 8 | 5 | 0 | 0 | 0 | 538380 | 617610 | 381980 |
| VKORC1L1 | 0 | 0 | 0 | 2 | 2 | 3 | 0 | 0 | 0 | 422830 | 456040 | 640010 |
| MTA2 | 0 | 0 | 0 | 7 | 7 | 6 | 0 | 0 | 0 | 508650 | 486910 | 520700 |
| PES1 | 0 | 0 | 0 | 6 | 5 | 5 | 0 | 0 | 0 | 411070 | 527350 | 514970 |
| EIF3I | 0 | 0 | 0 | 4 | 3 | 3 | 0 | 0 | 0 | 512160 | 458320 | 451010 |
| ATIC | 0 | 0 | 0 | 6 | 8 | 5 | 0 | 0 | 0 | 391840 | 617070 | 403100 |
| ATP13A1 | 0 | 0 | 0 | 10 | 14 | 10 | 0 | 0 | 0 | 371120 | 552310 | 482400 |
| QARS | 0 | 0 | 0 | 9 | 10 | 9 | 0 | 0 | 0 | 543900 | 477290 | 382590 |
| MRPS34 | 0 | 0 | 0 | 2 | 2 | 3 | 0 | 0 | 0 | 383010 | 431100 | 572490 |
| SRPRB | 0 | 0 | 0 | 5 | 3 | 4 | 0 | 0 | 0 | 540490 | 387680 | 439590 |
| ALG1 | 0 | 0 | 0 | 3 | 3 | 2 | 0 | 0 | 0 | 465700 | 453720 | 444450 |
| CLTC | 0 | 0 | 0 | 13 | 18 | 14 | 0 | 0 | 0 | 413940 | 533670 | 412010 |
| AAAS | 0 | 0 | 0 | 4 | 3 | 3 | 0 | 0 | 0 | 494210 | 486020 | 375370 |
| TMX1 | 0 | 0 | 0 | 2 | 2 | 2 | 0 | 0 | 0 | 458090 | 419880 | 468230 |
| VAPB | 0 | 0 | 0 | 2 | 4 | 3 | 0 | 0 | 0 | 452280 | 456380 | 421890 |
| TARDBP | 0 | 0 | 0 | 2 | 3 | 2 | 0 | 0 | 0 | 447900 | 557900 | 320170 |
| TFRC | 0 | 0 | 0 | 7 | 10 | 5 | 0 | 0 | 0 | 366190 | 603550 | 355420 |
| GART | 0 | 0 | 0 | 3 | 6 | 3 | 0 | 0 | 0 | 363210 | 586740 | 368870 |
| DDX58 | 0 | 0 | 0 | 9 | 12 | 8 | 0 | 0 | 0 | 416120 | 479030 | 421120 |
| SRP68 | 0 | 0 | 0 | 5 | 5 | 5 | 0 | 0 | 0 | 386510 | 419410 | 473500 |
| EPRS | 0 | 0 | 0 | 13 | 8 | 14 | 0 | 0 | 0 | 469100 | 310210 | 498910 |

| | | | | | | | | | | | |
|---|---|---|---|---|---|---|---|---|---|---|---|
| PGM1 | 0 | 0 | 0 | 6 | 7 | 3 | 0 | 0 | 0 | 498120 | 519760 | 252290 |
| COPB1 | 0 | 0 | 0 | 5 | 9 | 8 | 0 | 0 | 0 | 305290 | 511490 | 437610 |
| ACP1 | 0 | 0 | 0 | 2 | 2 | 2 | 0 | 0 | 0 | 427600 | 432680 | 392630 |
| OASL | 0 | 0 | 0 | 3 | 5 | 5 | 0 | 0 | 0 | 346240 | 391940 | 511650 |
| PAFAH1B1 | 0 | 0 | 0 | 3 | 2 | 3 | 0 | 0 | 0 | 397690 | 376490 | 469260 |
| NUP54 | 0 | 0 | 0 | 4 | 5 | 4 | 0 | 0 | 0 | 262490 | 501330 | 464080 |
| NCKAP1 | 0 | 0 | 0 | 9 | 7 | 8 | 0 | 0 | 0 | 387420 | 332640 | 481930 |
| MCM7 | 0 | 0 | 0 | 7 | 7 | 6 | 0 | 0 | 0 | 379750 | 429170 | 385620 |
| MMTAG2 | 0 | 0 | 0 | 2 | 2 | 2 | 0 | 0 | 0 | 324980 | 423130 | 441290 |
| HM13 | 0 | 0 | 0 | 3 | 2 | 2 | 0 | 0 | 0 | 383500 | 242850 | 537010 |
| TUBGCP3 | 0 | 0 | 0 | 5 | 6 | 7 | 0 | 0 | 0 | 214920 | 543860 | 346260 |
| NOP58 | 0 | 0 | 0 | 3 | 2 | 3 | 0 | 0 | 0 | 409430 | 276120 | 418370 |
| FAM120A | 0 | 0 | 0 | 7 | 9 | 6 | 0 | 0 | 0 | 357140 | 426510 | 289410 |
| EIF3G | 0 | 0 | 0 | 3 | 2 | 4 | 0 | 0 | 0 | 480560 | 243510 | 346340 |
| NHP2L1 | 0 | 0 | 0 | 2 | 2 | 2 | 0 | 0 | 0 | 212840 | 431760 | 420780 |
| ZMPSTE24 | 0 | 0 | 0 | 2 | 3 | 2 | 0 | 0 | 0 | 163500 | 435780 | 456140 |
| EIF3C | 0 | 0 | 0 | 4 | 6 | 5 | 0 | 0 | 0 | 342130 | 357380 | 330580 |
| NOC2L | 0 | 0 | 0 | 5 | 4 | 3 | 0 | 0 | 0 | 470430 | 343830 | 208490 |
| DDX47 | 0 | 0 | 0 | 2 | 4 | 4 | 0 | 0 | 0 | 202600 | 366920 | 452680 |
| OXA1L | 0 | 0 | 0 | 2 | 2 | 2 | 0 | 0 | 0 | 253860 | 314760 | 409340 |
| PON2 | 0 | 0 | 0 | 2 | 2 | 3 | 0 | 0 | 0 | 226890 | 208530 | 542430 |
| PHGDH | 0 | 0 | 0 | 3 | 3 | 2 | 0 | 0 | 0 | 256680 | 393580 | 316250 |
| TUBB2A | 0 | 0 | 0 | 2 | 2 | 2 | 0 | 0 | 0 | 361580 | 245290 | 357160 |
| PSMD12 | 0 | 0 | 0 | 3 | 4 | 2 | 0 | 0 | 0 | 335960 | 388940 | 231720 |
| HP1BP3 | 0 | 0 | 0 | 4 | 3 | 4 | 0 | 0 | 0 | 362610 | 229480 | 354070 |
| NCAPD2 | 0 | 0 | 0 | 9 | 11 | 10 | 0 | 0 | 0 | 296120 | 291550 | 340880 |
| PICALM | 0 | 0 | 0 | 3 | 4 | 2 | 0 | 0 | 0 | 378700 | 387900 | 158960 |
| XPO7 | 0 | 0 | 0 | 7 | 8 | 8 | 0 | 0 | 0 | 273340 | 314840 | 318770 |
| FAR1 | 0 | 0 | 0 | 3 | 3 | 3 | 0 | 0 | 0 | 280560 | 330050 | 292070 |
| ALDH18A1 | 0 | 0 | 0 | 6 | 6 | 5 | 0 | 0 | 0 | 298960 | 335370 | 266750 |
| KRT18 | 0 | 0 | 0 | 2 | 3 | 2 | 0 | 0 | 0 | 334490 | 187190 | 372670 |
| UBE3C | 0 | 0 | 0 | 6 | 6 | 8 | 0 | 0 | 0 | 313180 | 269080 | 310760 |
| ACSL3 | 0 | 0 | 0 | 4 | 3 | 4 | 0 | 0 | 0 | 323920 | 213480 | 355250 |
| EMC1 | 0 | 0 | 0 | 3 | 5 | 5 | 0 | 0 | 0 | 229620 | 348460 | 313790 |
| TNPO3 | 0 | 0 | 0 | 6 | 2 | 3 | 0 | 0 | 0 | 427880 | 198850 | 264720 |
| PTPN1 | 0 | 0 | 0 | 3 | 4 | 3 | 0 | 0 | 0 | 176050 | 376890 | 337420 |
| EIF2AK2 | 0 | 0 | 0 | 2 | 3 | 4 | 0 | 0 | 0 | 133570 | 258550 | 480940 |
| STAT3 | 0 | 0 | 0 | 6 | 4 | 5 | 0 | 0 | 0 | 305600 | 262770 | 302200 |
| TMCC3 | 0 | 0 | 0 | 3 | 4 | 3 | 0 | 0 | 0 | 250410 | 326220 | 289010 |
| MX2 | 0 | 0 | 0 | 3 | 5 | 5 | 0 | 0 | 0 | 238910 | 260910 | 332880 |

| | | | | | | | | | | | |
|---|---|---|---|---|---|---|---|---|---|---|---|
| AGK | 0 | 0 | 0 | 2 | 2 | 2 | 0 | 0 | 0 | 309770 | 315010 | 202350 |
| GNAS | 0 | 0 | 0 | 2 | 2 | 2 | 0 | 0 | 0 | 270180 | 290250 | 266290 |
| PRPF6 | 0 | 0 | 0 | 6 | 8 | 6 | 0 | 0 | 0 | 254540 | 298500 | 269930 |
| RAB32 | 0 | 0 | 0 | 2 | 2 | 2 | 0 | 0 | 0 | 261540 | 294150 | 264180 |
| ABHD16A | 0 | 0 | 0 | 4 | 6 | 3 | 0 | 0 | 0 | 274240 | 340920 | 195400 |
| SUN1 | 0 | 0 | 0 | 4 | 6 | 6 | 0 | 0 | 0 | 220590 | 262140 | 313130 |
| POR | 0 | 0 | 0 | 5 | 4 | 5 | 0 | 0 | 0 | 294360 | 237420 | 255110 |
| POM121C | 0 | 0 | 0 | 5 | 3 | 5 | 0 | 0 | 0 | 274120 | 146410 | 353650 |
| PDLIM7 | 0 | 0 | 0 | 3 | 3 | 4 | 0 | 0 | 0 | 204870 | 211610 | 354360 |
| TMX2 | 0 | 0 | 0 | 2 | 2 | 2 | 0 | 0 | 0 | 245750 | 257090 | 241100 |
| TBL2 | 0 | 0 | 0 | 3 | 4 | 5 | 0 | 0 | 0 | 261440 | 177920 | 281600 |
| GOT1 | 0 | 0 | 0 | 3 | 2 | 2 | 0 | 0 | 0 | 323500 | 156620 | 216090 |
| NCEH1 | 0 | 0 | 0 | 2 | 3 | 3 | 0 | 0 | 0 | 181980 | 236430 | 268060 |
| SEC23A | 0 | 0 | 0 | 2 | 2 | 6 | 0 | 0 | 0 | 158580 | 150070 | 371560 |
| GPS1 | 0 | 0 | 0 | 3 | 2 | 2 | 0 | 0 | 0 | 193770 | 252240 | 230870 |
| AP2A1 | 0 | 0 | 0 | 5 | 6 | 7 | 0 | 0 | 0 | 202970 | 187930 | 267690 |
| G6PD | 0 | 0 | 0 | 3 | 2 | 2 | 0 | 0 | 0 | 200970 | 141450 | 296550 |
| NAE1 | 0 | 0 | 0 | 2 | 3 | 2 | 0 | 0 | 0 | 158510 | 314320 | 163630 |
| TUBGCP2 | 0 | 0 | 0 | 4 | 3 | 4 | 0 | 0 | 0 | 215700 | 174910 | 235770 |
| IPO5 | 0 | 0 | 0 | 6 | 5 | 5 | 0 | 0 | 0 | 296340 | 121440 | 180280 |
| KLHL12 | 0 | 0 | 0 | 3 | 2 | 3 | 0 | 0 | 0 | 155300 | 221270 | 221020 |
| RNH1 | 0 | 0 | 0 | 4 | 3 | 3 | 0 | 0 | 0 | 256640 | 125780 | 214270 |
| ERO1L | 0 | 0 | 0 | 2 | 2 | 3 | 0 | 0 | 0 | 234220 | 142110 | 210360 |
| ACAD9 | 0 | 0 | 0 | 4 | 2 | 3 | 0 | 0 | 0 | 215900 | 113810 | 252730 |
| MARS | 0 | 0 | 0 | 2 | 3 | 5 | 0 | 0 | 0 | 85068 | 163580 | 331810 |
| SEC63 | 0 | 0 | 0 | 4 | 3 | 3 | 0 | 0 | 0 | 208380 | 197860 | 171230 |
| OAS2 | 0 | 0 | 0 | 3 | 2 | 2 | 0 | 0 | 0 | 288190 | 238350 | 42586 |
| RECQL | 0 | 0 | 0 | 3 | 3 | 3 | 0 | 0 | 0 | 204550 | 172470 | 168740 |
| TMEM214 | 0 | 0 | 0 | 2 | 4 | 3 | 0 | 0 | 0 | 137120 | 229290 | 170990 |
| EIF3D | 0 | 0 | 0 | 2 | 2 | 2 | 0 | 0 | 0 | 216290 | 105960 | 195540 |
| LRRC40 | 0 | 0 | 0 | 2 | 4 | 2 | 0 | 0 | 0 | 114830 | 262960 | 133830 |
| KIAA0196 | 0 | 0 | 0 | 6 | 7 | 6 | 0 | 0 | 0 | 218670 | 159230 | 133500 |
| TOR4A | 0 | 0 | 0 | 2 | 4 | 2 | 0 | 0 | 0 | 122500 | 259400 | 122390 |
| DDX19A | 0 | 0 | 0 | 2 | 3 | 3 | 0 | 0 | 0 | 147800 | 180840 | 163790 |
| ANXA6 | 0 | 0 | 0 | 3 | 3 | 3 | 0 | 0 | 0 | 168910 | 134360 | 177230 |
| IGF2BP2 | 0 | 0 | 0 | 2 | 3 | 3 | 0 | 0 | 0 | 111140 | 105940 | 260830 |
| ZW10 | 0 | 0 | 0 | 3 | 4 | 3 | 0 | 0 | 0 | 139310 | 182190 | 156230 |
| ANXA11 | 0 | 0 | 0 | 2 | 2 | 2 | 0 | 0 | 0 | 131180 | 110210 | 231290 |
| AP1G1 | 0 | 0 | 0 | 2 | 2 | 4 | 0 | 0 | 0 | 139610 | 165220 | 131100 |
| PAK2 | 0 | 0 | 0 | 2 | 3 | 3 | 0 | 0 | 0 | 67339 | 138540 | 212320 |

| | | | | | | | | | | | |
|---|---|---|---|---|---|---|---|---|---|---|---|
| DYNC1LI1 | 0 | 0 | 0 | 2 | 2 | 2 | 0 | 0 | 0 | 143770 | 141360 | 131090 |
| SEC24C | 0 | 0 | 0 | 2 | 3 | 3 | 0 | 0 | 0 | 125650 | 125190 | 157430 |
| TELO2 | 0 | 0 | 0 | 4 | 3 | 4 | 0 | 0 | 0 | 160350 | 110840 | 120170 |
| MYO1E | 0 | 0 | 0 | 3 | 4 | 5 | 0 | 0 | 0 | 106610 | 122340 | 150110 |
| PCID2 | 0 | 0 | 0 | 2 | 3 | 3 | 0 | 0 | 0 | 108770 | 100790 | 164250 |
| USO1 | 0 | 0 | 0 | 2 | 5 | 3 | 0 | 0 | 0 | 72602 | 204980 | 80935 |
| TBCD | 0 | 0 | 0 | 2 | 6 | 5 | 0 | 0 | 0 | 33511 | 139460 | 170090 |
| WFS1 | 0 | 0 | 0 | 2 | 2 | 2 | 0 | 0 | 0 | 124930 | 94586 | 118210 |
| NPEPPS | 0 | 0 | 0 | 2 | 3 | 2 | 0 | 0 | 0 | 84219 | 128780 | 94134 |
| EXOC4 | 0 | 0 | 0 | 2 | 3 | 3 | 0 | 0 | 0 | 88863 | 96864 | 113410 |
| DCTN1 | 0 | 0 | 0 | 2 | 2 | 2 | 0 | 0 | 0 | 102510 | 61673 | 97020 |
| SAMD9 | 0 | 0 | 0 | 3 | 4 | 4 | 0 | 0 | 0 | 66456 | 88167 | 96438 |
| PSMD5 | 0 | 0 | 0 | 2 | 2 | 2 | 0 | 0 | 0 | 55123 | 79879 | 107540 |
| FLNA | 0 | 0 | 0 | 4 | 6 | 5 | 0 | 0 | 0 | 59594 | 79548 | 96120 |
| PLEC | 0 | 0 | 0 | 9 | 7 | 11 | 0 | 0 | 0 | 70849 | 42336 | 114330 |
| XPO6 | 0 | 0 | 0 | 2 | 3 | 2 | 0 | 0 | 0 | 77047 | 107670 | 40856 |
| RARS2 | 0 | 0 | 0 | 2 | 2 | 2 | 0 | 0 | 0 | 111510 | 42462 | 55471 |
| KIF5B | 0 | 0 | 0 | 2 | 3 | 3 | 0 | 0 | 0 | 49604 | 68717 | 76528 |
| VPS51 | 0 | 0 | 0 | 2 | 2 | 2 | 0 | 0 | 0 | 103040 | 46976 | 42454 |
| KIAA1524 | 0 | 0 | 0 | 2 | 3 | 2 | 0 | 0 | 0 | 54855 | 74574 | 53827 |
| KIAA1033 | 0 | 0 | 0 | 2 | 3 | 2 | 0 | 0 | 0 | 36330 | 86521 | 21366 |
| GCN1L1 | 0 | 0 | 0 | 3 | 2 | 5 | 0 | 0 | 0 | 35162 | 21426 | 62894 |
| RANBP2 | 0 | 0 | 0 | 2 | 4 | 3 | 0 | 0 | 0 | 17896 | 36344 | 26198 |

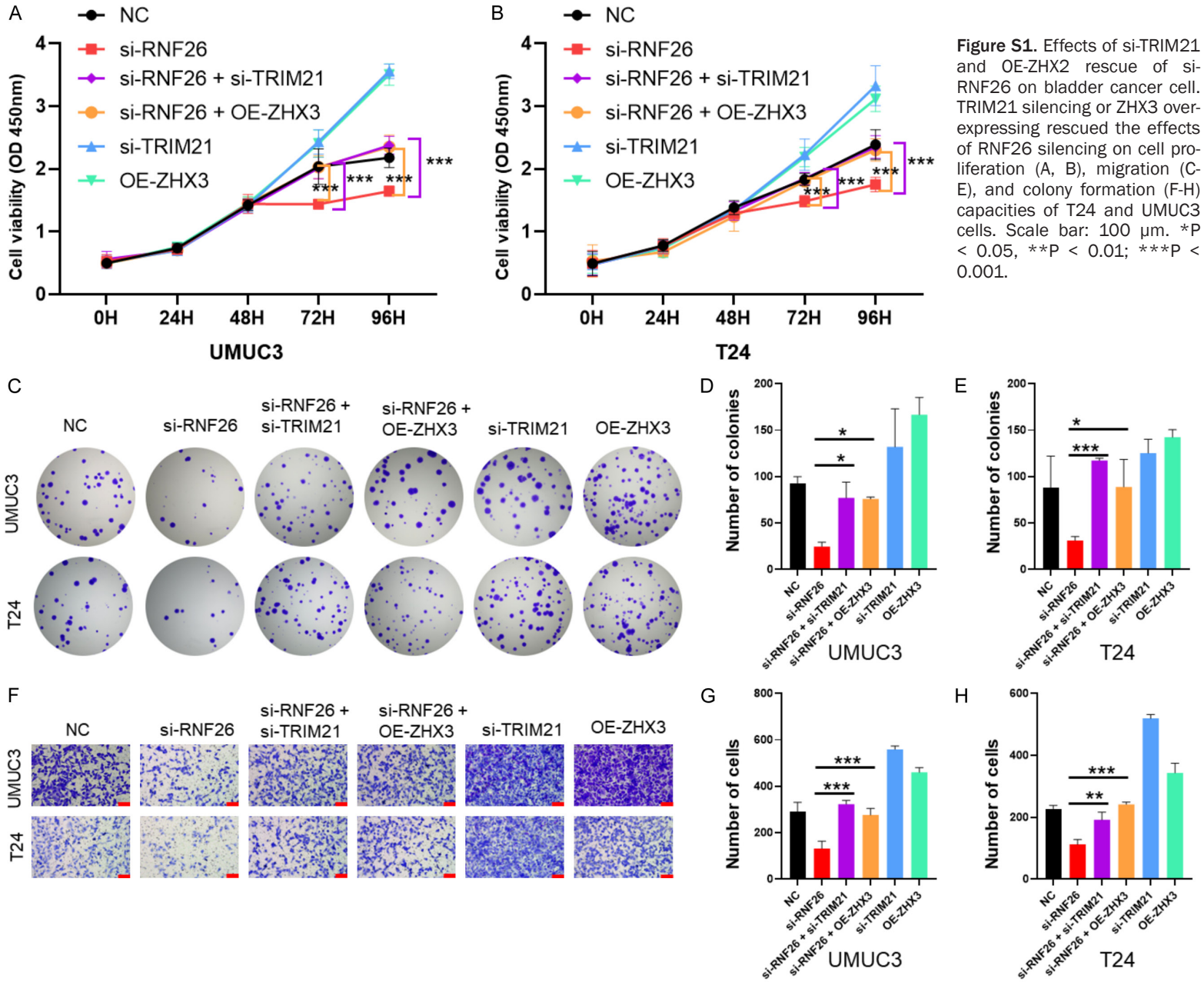


**Figure S1.** Effects of si-TRIM21 and OE-ZHX2 rescue of si-RNF26 on bladder cancer cell. TRIM21 silencing or ZHX3 over-expressing rescued the effects of RNF26 silencing on cell proliferation (A, B), migration (C-E), and colony formation (F-H) capacities of T24 and UMUC3 cells. Scale bar: 100 μm. *P < 0.05, **P < 0.01; ***P < 0.001.